Chapter 2
Theories and Models of Ion Diffusion

This chapter describes some models that are often used in trying to understand experimental data and fundamental questions in ion diffusion in ionically conducting materials. The basics of linear response theory are introduced first, with the definition of the linear response function, the Kramers-Kronig relations, and the Fluctuation-Dissipation theorem. The second section is devoted to present the Debye model and several other phenomenological descriptions of dielectric relaxation in materials whose electrical response is dominated by bound charges. This helps to understand the conductivity relaxation that occurs in materials with mobile charges like ionic conductors, and to introduce the so called conductivity formalism and electric modulus formalism for the analysis of experimental data of ion diffusion dynamics. A simple model of ion hopping is introduced that accounts for the thermally activated behavior often found in ionic conductivity data. The relationship between non-Debye relaxation and non-Gaussianity of the dynamics in the real space is also discussed in this chapter. Finally, three different models for ion diffusion are described in some detail. These are the Random Barrier Model, the MIGRATION concept, and the Coupling Model.

2.1 Linear Response Theory

In physics and material science we often encounter the problem of understanding, and even predicting how the system of interest will respond when an external force or perturbation is applied to drive it away from equilibrium. Response theory is devoted to this goal [1]. For example, if a temperature gradient is applied to a material, the response is heat transport through it, and this response is determined by the thermal conductivity of the material. Or when we apply an electric field as an external force to the same material, the free electrical charges will flow and give

© Springer International Publishing Switzerland 2017

J. Habasaki et al., *Dynamics of Glassy, Crystalline and Liquid Ionic Conductors*,
Topics in Applied Physics 132, DOI 10.1007/978-3-319-42391-3_2

rise to a current density in response. The magnitude of the current density is determined by the electrical conductivity of the material, and, if the response is *linear*, the current density will be proportional to the magnitude of the applied electric field.

We may be interested in the *stationary* response of the system when applying a time independent external force on it, or in the *transient* response of the system. The latter is how the system evolves with time to reach a stationary state under a time independent external force or, conversely how it returns to equilibrium with time after the external force is removed. We may be also interested in the response of the system if the applied external force is time dependent. In this case, if the response is *linear*, we can use Fourier analysis to obtain the response of the system as a superposition of the responses to sine waves of different frequencies that are the Fourier components of the time dependent applied force. This is why the study of the response of a system at different frequencies is relevant. In the following, we shall present a general introduction to linear response theory, and then specialize it to the case of ionically conducting materials.

2.1.1 Linear Response Function

Let us consider a small perturbation or external force $x(t)$ acting on an isotropic system in causing a response $y(t)$. If we assume *linearity* (i.e. the reaction of the system to the sum of two different perturbations is the sum of the two reactions separately to each perturbation) and *causality* (that is, only forces applied in the past contribute to the response at a given time t), the response can be related to the perturbation by [2]:

$$y(t) = \int_{-\infty}^{t} J(t-t')\frac{dx(t')}{dt'}dt', \tag{2.1a}$$

where $J(\tau)$ is known as the material function. This material equation is often written also as

$$y(t) = y_{\infty} + \int_{-\infty}^{t} J(t-t')\frac{dx(t')}{dt'}dt', \tag{2.1b}$$

where the magnitude y_{∞} accounts for the instantaneous response of the system (or its response for very short times, entirely due to fast processes, which are not related to the response from processes that we are interested in, and may not be accessible by experiment). The material function can be determined by measuring the response of the system to a step-like perturbation, $x(t) = x_0$ for $t \geq 0$ and

$x(t) = 0$ before. In this case, $dx(t)/dt = x_0\delta(t)$, with $\delta(t)$ the delta function, and substituting in Eq. (2.1b) we obtain the material function $J(t) = [y(t) - y_\infty]/x_0$. Equation (2.1a) describes the response of the system as a convolution of the material function with the time derivative of the applied external force. Note that the time dependence of the system only depends on the time interval between the application of the force and the observation time t. We can then define a time interval, $\tau = t - t'$, and write Eq. (2.1a) as

$$y(t) = \int_0^\infty J(\tau)\frac{dx(t-\tau)}{d\tau}d\tau, \tag{2.1c}$$

Partial integration of Eq. (2.1c) results in the following alternative expression relating the response and the external force signals in the time domain:

$$y(t) = \int_0^\infty \frac{dJ(\tau)}{d\tau}x(t-\tau)d\tau = \int_0^\infty R(\tau)x(t-\tau)d\tau, \tag{2.1d}$$

where $R(\tau) = dJ(\tau)/d\tau$ is the so-called response function (linear response function, or impulse response function). This means that, in general, the value of $y(t)$ will depend not only on the present value of $x(t)$, but also on past values, and we can approximate $y(t)$ as a weighted sum of the previous values of $x(t-\tau)$, with the weights given by the response function $R(\tau)$. Note that for an impulse or delta function perturbation, $x(t) = x_0\delta(t)$, the response of a system will be proportional to the (impulse) response function, $y(t) = x_0R(t)$.

By inverting Eq. (2.1) we obtain:

$$x(t) = \int_{-\infty}^t G(t-t')\frac{dy(t')}{dt'}dt', \tag{2.2}$$

where $x(t)$ and $y(t)$ are a pair of conjugated variables. If $y(t)$ is an extensive quantity, the material function $J(\tau)$ is a generalized compliance, and the time dependent process is defined as retardation. If $y(t)$ is an intensive quantity, the material function $G(\tau)$ is a generalized modulus, and the time dependent process is relaxation. It follows from Eqs. (2.1) and (2.2) that

$$\int_{-\infty}^\infty J(t-t')G(t')dt' = \delta(t). \tag{2.3a}$$

$$J^*(\omega)G^*(\omega) = 1. \tag{2.3b}$$

Equation (2.3b) is obtained by Fourier transformation of Eq. (2.3a) and relates the complex functions $J^*(\omega)$ and $G^*(\omega)$ in the frequency domain. If we are interested in relating the response of the system to the external perturbation as a function of frequency, we consider a stationary periodic time dependent perturbation of the form, $x(t) = x_0 e^{-j\omega t}$, where ω is the angular frequency. We obtain by Fourier transform both sides of Eq. (2.1d) that

$$\int_{-\infty}^{\infty} y(t) e^{-j\omega t} dt = \int_{-\infty}^{\infty} \left[\int_{0}^{\infty} R(\tau) x(t-\tau) d\tau \right] e^{-j\omega t} dt, \tag{2.4a}$$

$$\int_{-\infty}^{\infty} y(t) e^{-j\omega t} dt = \int_{-\infty}^{\infty} x(t') e^{-j\omega t'} dt \int_{0}^{\infty} R(\tau) e^{-j\omega \tau} d\tau, \tag{2.4b}$$

with $t' = t - \tau$. The quantities, x (ω) and $y(\omega)$, which are respectively the Fourier transforms of $x(t)$ and $y(t)$, satisfies the relation,

$$y^*(\omega) = \chi^*(\omega)\, x^*(\omega), \tag{2.4c}$$

where the susceptibility function, $\chi^*(\omega)$, is the one-sided Fourier transform (Laplace transform) of the impulse response function, $R(\tau)$:

$$\chi^*(\omega) = \int_{0}^{\infty} R(\tau) e^{-j\omega \tau} d\tau. \tag{2.5}$$

While the impulse response function is real, the susceptibility is complex,

$$\chi^*(\omega) = \chi'(\omega) - j\chi''(\omega), \tag{2.6}$$

and the real and imaginary parts of the susceptibility can be obtained from the response function by

$$\chi'(\omega) = \int_{0}^{\infty} R(\tau) \cos \omega\tau \, d\tau, \tag{2.7a}$$

$$\chi''(\omega) = \int_{0}^{\infty} R(\tau) \sin \omega\tau \, d\tau. \tag{2.7b}$$

It follows straightforwardly from these relations that $\chi'(\omega)$ is an even function of frequency and $\chi''(\omega)$ is an odd function of frequency.

2.1.2 The Kramers-Kronig Relations

Since $\chi'(\omega)$ and $\chi''(\omega)$ are cosine and sine transforms of the same function, the real and imaginary parts of the susceptibility are not independent of each other. Provided that: (1) the response function is real and analytic, (2) the system response at a given time only depends on the forces applied before that time (causality), and (3) the susceptibility converges to zero stronger than $1/\omega$ at high frequencies (i.e. there is not time for the system to respond if the applied force oscillates at enough high frequencies), it can be shown that $\chi'(\omega)$ and $\chi''(\omega)$ are related by the Kramers-Kronig relationships [3–6]:

$$\chi'(\omega) = \frac{1}{\pi}\,\mathcal{P}\int_{-\infty}^{\infty}\frac{\chi''(\omega)}{\omega'-\omega}d\omega', \tag{2.8a}$$

$$\chi''(\omega) = -\frac{1}{\pi}\,\mathcal{P}\int_{-\infty}^{\infty}\frac{\chi'(\omega)}{\omega'-\omega}d\omega', \tag{2.8b}$$

where the symbol $\mathcal{P}$ denotes the Cauchy principal value. Usually valid in most physical situations, these relations show that the full susceptibility function can be obtained if we just know its real (or imaginary) part at every frequency. An alternate form for the Kramers-Kronig relations can be derived that involves only the response of the system at positive frequencies. If we multiply the numerator and denominator in Eq. (2.8) by $(\omega' + \omega)$ we obtain:

$$\chi'(\omega) = \frac{1}{\pi}\,\mathcal{P}\int_{-\infty}^{\infty}\frac{\omega'\chi''(\omega)}{\omega'^2-\omega^2}d\omega' + \frac{1}{\pi}\,\mathcal{P}\int_{-\infty}^{\infty}\frac{\omega\chi''(\omega)}{\omega'^2-\omega^2}d\omega', \tag{2.9a}$$

$$\chi''(\omega) = -\frac{1}{\pi}\,\mathcal{P}\int_{-\infty}^{\infty}\frac{\omega'\chi'(\omega)}{\omega'^2-\omega^2}d\omega' - \frac{1}{\pi}\,\mathcal{P}\int_{-\infty}^{\infty}\frac{\omega\chi'(\omega)}{\omega'^2-\omega^2}d\omega'. \tag{2.9b}$$

Since $\chi''(\omega)$ and $\chi'(\omega)$ are odd and even functions of frequency respectively, the second integral in Eq. (2.9a) and the first integral in Eq. (2.9b) vanish, and we can finally write:

$$\chi'(\omega) = \frac{2}{\pi}\mathcal{P}\int_{0}^{\infty}\frac{\omega'\chi''(\omega)}{\omega'^2-\omega^2}d\omega', \tag{2.10a}$$

$$\chi''(\omega) = -\frac{2}{\pi}\mathcal{P}\int_{0}^{\infty}\frac{\omega\chi'(\omega)}{\omega'^2-\omega^2}d\omega'. \tag{2.10b}$$

The imaginary part of the susceptibility function is out of phase with the applied force and therefore determines how energy is dissipated by the system. From the Kramers–Kronig relations we can conclude that it is sufficient to measure the dissipative response of a system in order to determine its in-phase response (and vice versa).

2.1.3 The Fluctuation-Dissipation Theorem

We can further examine the relationship between the susceptibility, or the linear response function, and the dissipation of energy in a system, by introducing the Fluctuation Dissipation Theorem (FDT) [7, 8]. The FDT is a general result of statistical thermodynamics that relates the microscopic fluctuations in a system at thermal equilibrium and the response of the macroscopic system to applied external perturbations. In other words, the FDT relates non-equilibrium dynamics of a system driven away from (or relaxing towards) equilibrium to the existing fluctuations and dynamics in the equilibrium state. The FDT thus allows the use of microscopic or molecular models to predict material properties in the context of linear response theory.

Thermodynamic quantities characterizing a macroscopic system are described in statistical physics by their average values. These quantities actually fluctuate around their mean value due to the stochastic motions of the particles in the system. For instance, for a given quantity $y(t)$ with average value, $\langle y \rangle$, the fluctuations of the quantity are defined as $\Delta y(t) = y(t) - \langle y \rangle$. The correlation function $\varphi(\tau)$ is introduced in order to describe the dependence of the fluctuations at a given time $\Delta y(t+\tau)$ on their value $\Delta y(t)$ at a previous time separated by the time interval τ, and it is defined as the average of the product of these two values of the fluctuations at two times separated by τ, $\varphi(\tau) = \langle \Delta y(t) \Delta y(t+\tau) \rangle$. In the case of a *stationary process* the time t is irrelevant and the correlation function can be written as:

$$\varphi(\tau) = \langle \Delta y(0) \Delta y(\tau) \rangle. \tag{2.11}$$

A normalized correlation function, $\phi(\tau) = \varphi(\tau)/\varphi(0)$, is often considered,

$$\phi(\tau) = \langle \Delta y(0) \Delta y(\tau) \rangle / \langle \Delta y(0) \Delta y(0) \rangle, \tag{2.12}$$

so that $\phi(0) = 1$. Note also that it is expected that the correlation function tends to zero for long enough τ, i.e. $\phi(\infty) = 0$.

It is worthwhile to emphasize that every correlation function of an observable quantity can be expressed in terms of the so-called memory function $K(t)$ by [9]

$$\frac{d\phi(t)}{dt} = -\int_0^t K(t-\tau)\phi(\tau)d\tau. \tag{2.13}$$

From the expression above, the time dependence of the correlation function is obtained if the memory function can be calculated by using a microscopic or molecular model or if the memory function can be described by an empirical function.

Again for the case of stationary processes, the so called spectral density function (or the power spectral density function, or simply the power spectrum), $S_y(\omega)$, is defined as the Fourier transform of the correlation function:

$$S_y(\omega) = \int_{-\infty}^{\infty} \varphi(\tau) e^{-j\omega\tau} d\tau. \tag{2.14}$$

The spectral density function is a measure of the frequency distribution of the fluctuations. It can be shown that the response function is related to the correlation function by:

$$R(\tau) = -\frac{1}{kT} \frac{d\varphi(\tau)}{d\tau}, \tag{2.15}$$

and therefore, the spectral density function in the classical limit (no quantum effects) is related to the imaginary part of the susceptibility by:

$$S_y(\omega) = \frac{2kT}{\omega} \chi''(\omega). \tag{2.16}$$

Within the approximations of the linear response theory, the Fluctuation Dissipation Theorem means that the relaxation dynamics of a macroscopic non-equilibrium disturbance is governed by the same mechanisms as the regression of spontaneous microscopic fluctuations in the equilibrium state [10, 11].

2.2 Dielectric Relaxation

Before analyzing relaxation dynamics driven by mobile ions in ionically conducting materials, it is instructive to describe the case of dielectric relaxation in materials with polarization charge. The dielectric relaxation that takes place in a dielectric material with bound electric charges at small electric field strengths can be analyzed within the framework of the linear response theory. In dielectrics the external perturbation is an applied electric field $E(t)$, and the response of the system is the polarization $P(t)$, or the electric displacement $D(t)$ [12]. Let us consider an isotropic system and a homogeneous electric field. We can then describe the time dependence of the magnitude of the polarization inside the material as:

$$P(t) = \varepsilon_0 \int_{-\infty}^{t} \chi(t - t')E(t')dt', \tag{2.17a}$$

$$P(t) = \varepsilon_0 \int_{0}^{\infty} \chi(\tau)E(t - \tau)d\tau, \tag{2.17b}$$

where $\chi(\tau)$ is the corresponding response function for the polarization and ε_0 the permittivity of a vacuum. Since the polarization is an intensive thermodynamic quantity, the function $\chi(\tau)$ is a generalized compliance. In the frequency domain, the polarization and the electric field are related through the complex dielectric susceptibility, $\chi^*(\omega)$, which is the one sided Fourier transform of $\chi(\tau)$ (see Eq. (2.5)), and

$$P^*(\omega) = \varepsilon_0 \chi^*(\omega) E^*(\omega). \tag{2.18}$$

Since the polarization can only depend on the electric field at previous times, a consequence of causality, the real and imaginary parts of the complex susceptibility must satisfy the Kramers–Kronig relations (see previous section).

Analogously, we can obtain the following relation between the electric displacement, D, and the electric field amplitudes if the electric field oscillates periodically at a given frequency, by using the complex dielectric permittivity, $\varepsilon^*(\omega) = 1 + \chi^*(\omega)$,

$$D^*(\omega) = \varepsilon_0 E^*(\omega) + P^*(\omega) = \varepsilon_0 \varepsilon^*(\omega)\, E^*(\omega). \tag{2.19}$$

Note that the frequency dependence of the susceptibility leads to frequency dependence of the permittivity, and characterizes the *dispersion* properties of the material.

2.2.1 Debye Relaxation

Debye theory of dielectric relaxation is the simplest model of rotational Brownian motion of spherical dipoles in a viscous medium where inertia effects are neglected [13, 14]. In this case it is found that the response function has the exponential time dependence. The same behaviour can be explained by assuming that, in the absence of an electric field, if there exists a polarization due to the occurrence of a field in the past, the decrease rate of the polarization at a given instant is independent of the history of the material and depends only on the value of the polarization at that instant, with which it is proportional. The proportionality constant has the

dimension of a reciprocal time and is often denoted by $1/\tau_D$, giving rise to the following first order differential equation:

$$-dP(t)/dt = P(t)/\,\tau_D, \tag{2.20}$$

the solution of which is

$$P(t) = P(0)e^{-t/\,\tau_D}. \tag{2.21}$$

It follows that the impulse response function can be written as

$$\chi(t) = \frac{1}{\tau} e^{-t/\,\tau_D}, \tag{2.22}$$

with τ_D the so called (Debye) relaxation time (see Fig. 2.1). The frequency dependence of the complex dielectric permittivity is given by

$$\varepsilon^*(\omega) = \varepsilon_\infty + \frac{\Delta\varepsilon}{1 + j\omega\tau_D}\ . \tag{2.23}$$

Figure 2.2 shows the frequency dependence of the real and imaginary parts of the dielectric permittivity of a system with a Debye relaxation. It can be observed that the real part shows an increase of $\Delta\varepsilon$ with decreasing frequency below the characteristic frequency $\omega_D = 1/\tau_D$, while the imaginary part shows a symmetric peak with the maximum at ω_D. The relaxation time is usually found to be thermally

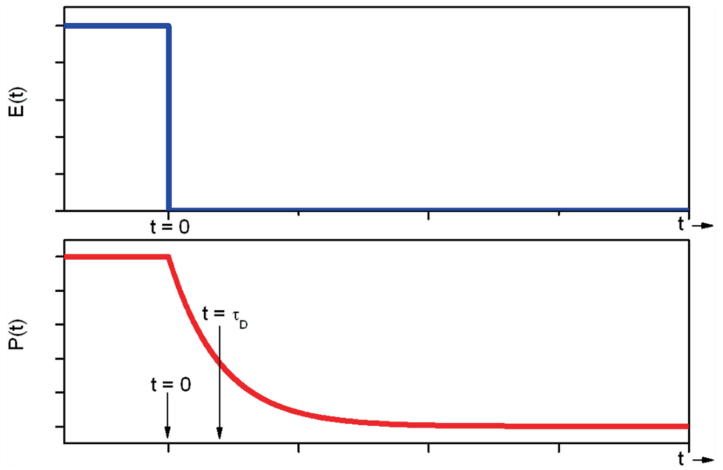

Fig. 2.1 Sketch showing the exponential time dependence of the polarization P(t) for an ideal Debye relaxation in a dielectric material. The polarization starts to decrease after removing the application of an external electric field, E(t), at t = 0. The time τ_D is the Debye relaxation time (see text)

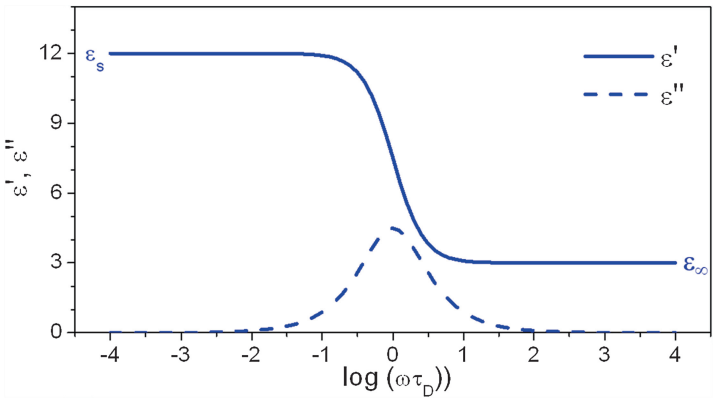

Fig. 2.2 Sketch of the frequency dependence of the real and imaginary parts of the dielectric permittivity ($\varepsilon^* = \varepsilon' - j\varepsilon''$) for a dielectric material showing a Debye relaxation with relaxation time τ_D. The values of the real part of the dielectric permittivity at low and high frequencies are taken as $\varepsilon_s = 12$ and $\varepsilon_\infty = 3$, respectively

activated, which can be explained in terms of a potential barrier for the dipoles to rotate in the system [2].

Within the framework of the memory function formalism (see Eq. (2.13)), the Debye relaxation is obtained by using

$$K(t-\tau) = \frac{\delta(t-\tau)}{\tau_D}, \tag{2.24}$$

which implies that the orientational rotations of the electric dipoles are random and uncorrelated (independent) events in the Debye relaxation model and characterized by one and the same relaxation time.

2.2.2 Non-Debye Relaxation

Although the Debye model provides a simple understanding of the relaxation phenomena, in most cases the measured dielectric relaxation spectra is more complex and show departures from the behavior expected from Eq. (2.23). In particular, it is usually found that the relaxation peak in the imaginary part of the susceptibility or dielectric permittivity functions is asymmetric and broader than expected for a Debye response. This behaviour is known as non-Debye (or sometimes non-ideal) dielectric relaxation. While the ultimate reason for the observed non-Debye relaxation is still a matter of scientific debate and may be different for different systems, there are usually two different approaches in the several proposed models to account for the non-Debye response. One approach is based on considering that the individual dipole rotations are not independent but correlated, and the relaxation is thus the result of a cooperative

process such as that proposed by Adam and Gibbs from configurational entropy arguments [15]. Cooperative relaxation also arises from interaction between the relaxation units, and the many-body relaxation is dynamically heterogeneous [16–18]. The other approach relies on considering that the individual dipole rotations take place as random and independent events, and each can be described as true Debye-like process, but that they are characterized by different relaxation times due to an inhomogeneous or disordered environment in the system giving rise to an energy landscape.

While the validity of the different approaches or models for the dielectric relaxation remains a subject of scientific debate, the non-Debye response of the relaxation process is often described in terms of phenomenological functions either in the time or frequency domains which can be used to obtain information about the dynamics and eventually to discriminate between the different theoretical models. One of the most used empirical functions to describe a relaxation process from long time ago is the so-called Kohlrausch-Williams-Watts (KWW) function [19–22]. Its time dependence is a stretched exponential decay of the form

$$\phi(t) = e^{-(t/\ \tau_{KWW})^{\beta_{KWW}}} \tag{2.25}$$

for the correlation function. The exponent or stretching parameter β_{KWW} is a fractional number between 0 and 1, what leads to an asymmetric broadening of the susceptibility spectra compared to the case of an ideal Debye exponential decay ($\beta_{KWW} = 1$). The corresponding memory function for a correlation function of the KWW type can be estimated to be [2, 9]

$$K(t-\tau) = \frac{\delta(t-\tau)}{\zeta(\tau)}\ , \quad \text{with}\ \ \zeta(\tau) \sim {\tau_{KWW}}^{1-\beta_{KWW}}. \tag{2.26}$$

Since the KWW function usually represents experimental data quite well, there has been a long standing search for realistic models that lead to KWW behavior [23, 24]. In particular, Ngai's Coupling Model (CM) [25, 26] provides a physical basis for the KWW behavior in the relaxation of complex systems with many applications. It assumes that at short times, before a crossover time t_c of the order of a few picoseconds, the relaxing species are independent from each other, and this primitive relaxation process is Debye-like with a characteristic primitive relaxation time τ_0. The onset of cooperativity after t_c would give rise to the slowing down of the relaxation dynamics and the corresponding KWW behavior of the correlation function. The important relationship derived in the CM model,

$$\tau_{KWW} = \left[\tau_0 t_c^{(\beta_{KWW}-1)}\right]^{1/\beta_{KWW}} \tag{2.27}$$

between the primitive relaxation time τ_0 and the experimentally determined values of τ_{KWW} and β_{KWW} allows the experimental verification of the model [18].

While the KWW function allows for a fairly good description of many experimental relaxation data in the time domain, there are other important and widely used empirical descriptions of the relaxation processes that describe the susceptibility or permittivity function in the frequency domain. Among these empirical functions is the so called Havriliak-Negami function [27] which reads

$$\varepsilon^*(\omega) = \varepsilon_\infty + \frac{\Delta\varepsilon}{(1 + (j\omega\,\tau_{HN})^\alpha)^\beta}\ . \tag{2.28}$$

The fractional parameters α and β describe the symmetric ($\beta = 1$) or asymmetric ($\beta < 1$) broadening of the relaxation peak in the dielectric spectra. These parameters being less than 1 account for the experimentally observed fractional power-law frequency dependence of the dielectric permittivity, the so-called Jonscher's law or universal dielectric response [28], since the limiting behavior of the dielectric loss at low and high frequencies is given by $\varepsilon''(\omega) \sim \omega^\alpha$ and $\varepsilon''(\omega) \sim \omega^{-\alpha\beta}$ respectively. The memory function which leads to a relaxation behavior according to the Havriliak-Negami function can be approximated by [9]

$$K(t-\tau) = \frac{\Omega_0 \tau^{-\alpha}(t-\tau)^{\beta-2}}{\Gamma(\beta-1)}\quad . \tag{2.29}$$

The case $\beta = 1$ in the Havriliak-Negami function leads to the so-called Cole-Cole (CC) function [29],

$$\varepsilon^*(\omega) = \varepsilon_\infty + \frac{\Delta\varepsilon}{(1 + (j\omega\,\tau_{CC})^\alpha)}\ , \tag{2.30}$$

which describes the case of a symmetric relaxation spectra, with the dielectric loss given by $\varepsilon''(\omega) \sim \omega^\alpha$ and $\varepsilon''(\omega) \sim \omega^{-\alpha}$ in the limit of low and high frequencies respectively. It accounts for broader spectra compared to the Debye case, which is in fact the limiting case for $\alpha = 1$. Another phenomenological expression that is often used to describe relaxation spectra was given by Davidson and Cole [30]. The Cole-Davidson (CD) function reads

$$\varepsilon^*(\omega) = \varepsilon_\infty + \frac{\Delta\varepsilon}{(1 + j\omega\,\tau_{CD})^\beta}\ , \tag{2.31}$$

and results from setting the parameter $\alpha = 1$ in the HN function. Although there are other empirical descriptions of dielectric relaxation, the Havriliak-Negami, Cole-Cole and Cole-Davidson functions in the frequency domain, together with the KWW function in the time domain, are most often used in the literature to describe non-Debye relaxation spectra or response function [12].

2.3 Conductivity Relaxation

2.3.1 *Electric Modulus Formalism*

While in the case of dielectric relaxation the response of the system is due to bound electric charge, when analyzing conductivity relaxation dynamics in ionically conducting materials, it is important to bear in mind that it is driven by mobile electric charge carried by the ions. In this case the relaxation process is the decay of the electric field $E(t)$ inside the conductor after applying an electric displacement $D(t)$. Analogous to the description of dielectric relaxation, let us assume an isotropic system and a homogeneous electric displacement. If an ionic conductor is placed between the charged plates of a condenser at time $t=0$, the displacement vector can be described by a step-function with amplitude D_0. It gives rise to an electric field that causes the mobile ions to diffuse and accumulate, which results in an additional and opposite electric field that increases with time until the total electric field that mobile ions feel inside the material cancels out. Therefore, the electric field inside the ionic conductor decays with time (see Fig. 2.3), and we can describe the time dependence of this electric field after $t=0^+$ as:

$$E(t) = \frac{D_0}{\varepsilon_0 \varepsilon_\infty} \Phi(t), \tag{2.32}$$

where $\varepsilon_0\varepsilon_\infty$ is the "high frequency" value of the dielectric permittivity, and $E(t=0^+) = D_0/\varepsilon_0\varepsilon_\infty$. The "high frequency" permittivity accounts for all possible contributions to the decay of the electric field between $t=0$ and $t=0^+$ and always before the mobile ions start to move. Thus, the correlation function for the electric field relaxation due to mobile ions is given by $\Phi(t)$.

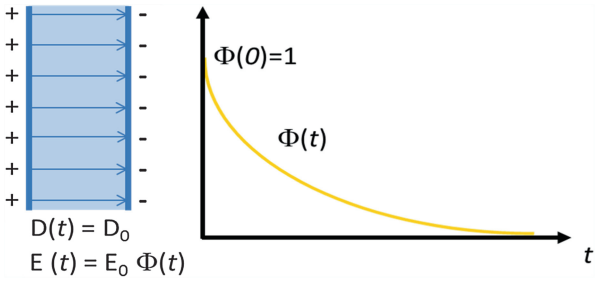

Fig. 2.3 Sketch showing the relaxation of the electric field inside an ionic conductor placed at time $t=0$ between the charged plates of a condenser where the displacement vector can be described by a step-function with amplitude D_0. The electric displacement gives rise to an electric field that causes the mobile ions to diffuse and accumulate, which results in an additional and opposite electric field that increases with time until the total electric field that mobile ions feel inside the material cancels out. The electric field inside the ionic conductor decays with time as $E(t) = E_0\Phi(t)$

By using the time derivative of Eq. (2.32) we can write

$$E(t) = \frac{1}{\varepsilon_0 \varepsilon_\infty} \left[D(t) + \int_{-\infty}^{t} \frac{d\Phi}{dt}(t - t') D(t') dt' \right] \tag{2.33a}$$

and therefore

$$E(t) = \frac{D_0}{\varepsilon_0 \varepsilon_\infty} \left[1 + \int_{0}^{t} \frac{d\Phi}{d\tau}(\tau) d\tau \right]. \tag{2.33b}$$

In the frequency domain, the relation between the electric field and the electric displacement is obtained by performing the Fourier transform of Eq. (2.33), resulting in

$$E^*(\omega) = \frac{\left[1 + \dot{\Phi}^*(\omega)\right]}{\varepsilon_0 \varepsilon_\infty} D^*(\omega). \tag{2.34}$$

where $\dot{\Phi}^*(\omega)$ accounts for the Fourier transform of the time-derivative of the correlation function describing the electric field relaxation. By using the electric modulus $M^*(\omega) = 1/\varepsilon^*(\omega)$ and Eq. (2.19) we can write

$$E^*(\omega) = \frac{M^*(\omega)}{\varepsilon_0} D^*(\omega), \tag{2.35}$$

and therefore

$$M^*(\omega) = M_\infty \left[1 + \dot{\Phi}^*(\omega)\right], \tag{2.36a}$$

$$M^*(\omega) = M_\infty \left[1 + \int_{0}^{\infty} \frac{d}{dt} \Phi(t) e^{-j\omega t} dt \right], \tag{2.36b}$$

where $M_\infty = 1/\varepsilon_\infty$. Equation (2.36) means that the correlation function $\Phi(t)$ for the time decay describing the relaxation of the electric field (often referred to as electrical conductivity relaxation), which is governed by the dynamics of the mobile ions, can be obtained from the electric modulus as a function of frequency. By using the relation $1 + \dot{\Phi}^*(\omega) = j\omega\Phi^*(\omega)$, we can relate the Fourier transform of the correlation function, $\Phi^*(\omega)$, to the experimental impedance spectra $Z^*(\omega) = 1/\sigma^*(\omega) = 1/j\omega\varepsilon_0\varepsilon^*(\omega) = M^*(\omega)/j\omega\varepsilon_0$ as

$$\Phi^*(\omega) = \varepsilon_0 \varepsilon_\infty Z^*(\omega) \tag{2.37}$$

2.3.2 Conductivity Formalism

Alternatively, we can think of the ion diffusion process in ionic conductors in terms of the successive jumps of the ions from their sites to neighboring empty sites in the structure. According to linear response theory, the frequency dependent complex electrical conductivity due to ion hopping is proportional to the Fourier transform of the current density autocorrelation function:

$$\sigma^*_{hop}(\omega) = \frac{V}{3k_BT}\int_0^\infty \langle J(0)J(t)\rangle e^{-j\omega t}dt\ , \tag{2.38}$$

where V is the volume of the sample, and k_B denotes Boltzmann's constant. The current density is given by

$$J(t) = \frac{1}{V}\sum_i q_i v_i(t) \tag{2.39}$$

with q_i and v_i the charge and velocity of the ion i and the sum performed for all the mobile ions in the sample. The combination of Eqs. (2.38–2.39) shows that the electrical conductivity is related to velocity correlation function of the hopping ions, $\left\langle \sum_{i,j} v_i(0)v_j(t) \right\rangle$, as

$$\sigma^*_{hop}(\omega) = \frac{q^2}{3Vk_BT}\int_0^\infty \left\langle \sum_{i,j} v_i(0)v_j(t) \right\rangle e^{-j\omega t}dt\ . \tag{2.40}$$

Similarly, the frequency dependence of the complex self-diffusion coefficient due to ion hopping is proportional to the Fourier transform of the velocity autocorrelation function:

$$D^*_{hop}(\omega) = \frac{1}{3}\int_0^\infty \langle v(0)v(t)\rangle e^{-j\omega t}dt\ , \tag{2.41}$$

and it is related to the complex electrical conductivity through the generalized Nernst-Einstein equation:

$$\sigma^*_{hop}(\omega) = \frac{Nq^2}{Vk_BT\,H^*(\omega)}D^*_{hop}(\omega), \tag{2.42}$$

with N the total number of mobile ions and $H^*(\omega)$ the so-called Haven ratio. When correlations between the velocities of different ions can be neglected, the velocity correlation function is proportional to the velocity autocorrelation function,

$$\left\langle \sum_{i,j} v_i(0)v_j(t) \right\rangle = N\langle v(0)v(t)\rangle \tag{2.43}$$

and the Haven ratio is real and equal to 1. But if cross correlations cannot be neglected, then the Haven ratio is a complex function of the frequency.

In the particular case that the ions behave as random walkers, they have no memory and their velocities are uncorrelated, so the velocity correlation function is proportional to a delta function at time $t = 0$,

$$\left\langle \sum_{i,j} v_i(0)v_j(t) \right\rangle_{random\ hops} = \frac{N\,\Gamma\,x_0^2}{2}\delta(t), \tag{2.44}$$

where, Γ and x_0 are the hopping rate and the elementary jump distance of the ions, respectively. Thus, random hopping yields a hopping conductivity which is real and constant that is given by

$$\sigma^*_{hop}(\omega) = \frac{n\,q^2\,x_0^2\,\Gamma}{6k_BT} = \frac{n\,q^2\,D_0}{k_BT} \tag{2.45}$$

with $n = N/V$ as the concentration of mobile ions, and a frequency independent diffusion coefficient given by $D_0 = \frac{x_0^2\,\Gamma}{6}$. However, experimental data usually shows a dispersive (frequency dependent) complex conductivity, which is interpreted in terms of the non-random nature of the ion hopping events. As in the case of dielectric relaxation, there are models that consider the dispersive behavior arises from the existence of a distribution of hopping rates because the different ions experience different environments at a given time, and other models where the dispersive conductivity is a consequence of the cooperative hopping of mobile ions due to ion-ion interactions.

It is important to remark that independently of using the conductivity or electric modulus formalism in order to analyze or interpret experimental data of the electrical response of ionic conductors, they are just different representations of the same data, that are related through

$$Z^*(\omega) = M^*(\omega)/j\omega\varepsilon_0 = 1/\sigma^*(\omega) = \frac{1}{\sigma^*_{hop}(\omega) + j\omega\varepsilon_0\varepsilon_\infty}, \tag{2.46}$$

and therefore contain the same information about ion dynamics.

2.3.3 *Empirical Description of Ion Dynamics. Distribution of Relaxation Times*

The experimental data of electrical conductivity relaxation (ECR) from admittance spectroscopy measurements can be represented in terms of the complex conductivity or the electric modulus. The two alternative representations of the

same data have proven to be very useful in the study of ion diffusion dynamics in ionically conducting materials [26, 31]. Similar to the case of dielectric relaxation in polarizable insulating materials, a Debye response function, i.e. exponential time decay with a single relaxation time, is rarely observed [32]. The usual behavior is a rather strongly non-Debye response, characterized by a frequency dispersive electrical conductivity and therefore by a broader, and usually asymmetric, peak in the imaginary part of the electric modulus spectra compared to that expected from a Debye relaxation. The observed departure from a simple Debye behavior in ECR has been mainly considered as due to either the presence of structural disorder and randomness in the material [33], or to the effect of interactions among ions in their cooperative motion [18, 34–37]. Before entering in the description of some of these models that have been proposed to explain the non-Debye character of the conductivity relaxation, we describe the main features of the relaxation in the frequency and time domains and an empirical approach to study the dynamics of mobile ions by using an analysis based on distributions of relaxation times. Although it is a mathematical tool, it may offer hints in the search of the physics behind the relaxation process. The ac conductivity $\sigma'(\omega)$ of these materials shows a constant value at low frequencies, the so called dc conductivity value, and a crossover to a power law dependence with frequency at high frequencies, so that the real part of the conductivity can be expressed as [28, 38, 39]

$$\sigma'(\omega) = \sigma_{dc} + A\omega^n \tag{2.47}$$

where σ_{dc} is the dc conductivity, A is a temperature dependent parameter and n is a fractional exponent which usually lies between 0.6 and 1 [28, 40]. This universal behavior is shown in Fig. 2.4. Equation (2.47) and Kramers-Kronig relations lead to a frequency dependence of the complex conductivity which can be written as

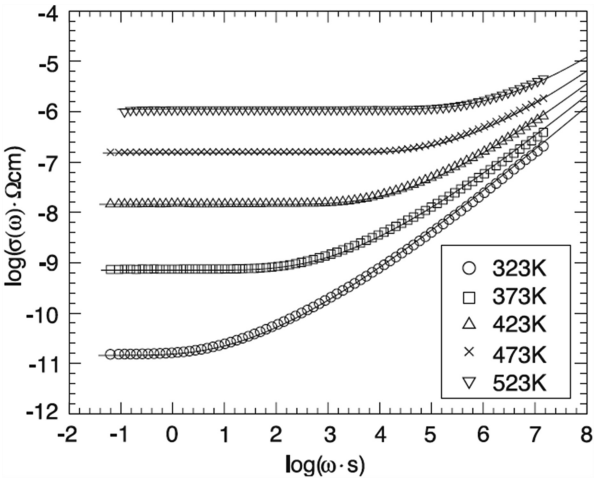

Fig. 2.4 Frequency dependent conductivity of a sodium germanate glass of composition $0.2Na_2O \cdot 0.8GeO_2$ at several temperatures. Reproduced from [41] with permission

$$\sigma^*(\omega) = \sigma_{dc}[1 + (j\omega/\omega_c)^n] + j\omega\varepsilon_0\varepsilon_\infty \tag{2.48a}$$

$$\sigma^*(\omega) = \sigma^*_{hop}(\omega) + j\omega\varepsilon_0\varepsilon_\infty \tag{2.48b}$$

where included is the high frequency permittivity term, $j\omega\varepsilon_0\varepsilon_\infty$, due to the contributions from all the polarization at higher frequencies, and ω_c represents a crossover frequency from the dc conductivity plateau (at $\omega < \omega_c$) to the power law frequency dependence (at $\omega > \omega_c$).

Some authors [42–44] have argued the advantage of using the $\sigma'(\omega)$ representation of the measurements since it allows to separate the hopping dynamics from the high frequency permittivity term due to other different physical processes occurring at shorter times. However, it is important to note that the characteristic crossover frequency characterizing ion hopping dynamics is always of the order of $\omega_c \approx \sigma_{dc}/\varepsilon_0\varepsilon_\infty$ [33, 45], which shows that in fact ion dynamics are influenced by the dielectric permittivity of the medium, in particular the time dependence of the corresponding correlation function. It is also relevant to point out that the physical significance arising from the additive character of the two contributions in Eq. (2.47) has been questioned [46–48]. Equation (2.47) implies that both terms contribute to the conductivity at all frequencies, like two independent conduction mechanisms simultaneously present at every time. And this is actually at odds with the finding of a crossover frequency proportional to the value of the dc conductivity ($\omega_c \approx \sigma_{dc}/\varepsilon_0\varepsilon_\infty$), and also with the fact that experimental data of the imaginary part of the complex conductivity do not usually increase indefinitely as the frequency decreases. However, Eq. (2.47) is widely used in the literature in order to describe empirical conductivity data of ionic conductors, since it describes rather well the conductivity spectra, $\sigma'(\omega)$, particularly in the limits of low and high frequencies.

An alternative description of ECR has been made in the time domain [49–52] in terms of electric field decay with the Kohlrausch-Williams-Watts (KWW) function [19–22]. As previously stated, at constant displacement vector, the electric field inside an ionic conductor shows a time decay $\Phi(t)$ well approximated by a KWW function or stretched exponential function,

$$\Phi(t) = e^{-(t/\,\tau^*)^{1-n}} \tag{2.49}$$

where τ^* is a temperature activated relaxation time and $0 < n < 1$. Although the physical significance of the KWW function is not generally agreed by researchers in the field, it has been interpreted in terms of the slowing of the relaxation process due to cooperative many-ion dynamics, with the parameter n as an index of correlations between the ions in motion. The case $n = 0$ would thus correspond to the completely uncorrelated ion motion giving rise to a Debye response characterized by exponential time decay function.

Experimental conductivity data are usually obtained in the frequency domain from Admittance Spectroscopy, and the time decay $\Phi(t)$ is calculated from the electric modulus data according to Eq. (2.36). The calculation of the decay

function, $\Phi(t)$, involves a numerical Fourier transform of the measured data in the frequency domain from which the parameters n and τ^* that best characterize the relaxation process by the KWW decay function can be obtained. However, it is well known that the calculation of the Fourier transform by numerical methods from real data in the frequency domain is affected by numerical errors arising from the fact that the experimental data set is usually discrete and finite. An alternative procedure has been proposed in order to calculate the time decay function without evaluating any numerical Fourier transform [52]. It consists of finding the coefficients g_i of a distribution of discrete relaxation times τ_i so that the measured frequency response may be approached as a superposition of Debye-like processes according to

$$\dot{\Phi}^*(\omega) \approx \sum_1^n g_i[1/(1 + j\omega\tau_i)] \tag{2.50}$$

The time decay function can then be calculated as

$$\Phi(t) \approx \sum_1^n g_i \exp(-t/\tau_i) \tag{2.51}$$

Assuming a KWW dependence for the time decay, one can fit the parameters n and τ^* describing the conductivity relaxation in the time domain. Other methods based on a complex non-linear least squares fitting of experimental data to equivalent circuit models [53–55] can also be used in order to obtain the time decay function from admittance spectroscopy data avoiding the numerical Fourier transform.

A different approach has been reported based on an analysis of the frequency dependence of the electric modulus. The electric modulus spectra in ionic conductors can be usually well described by one of the empirical relaxation functions in the frequency domain like the Cole-Cole, Cole-Davidson, or Havriliak-Negami. These functions, described in the subsection devoted to dielectric relaxation, can also be used to describe phenomenologically the electrical conductivity relaxation in ionic conductors [56]. The advantage is that an analytical expression exists for the distribution of relaxation times once the parameters characterizing the empirical function (CC, CD or HN) in the frequency domain is obtained. This procedure allows then a description of the decay function in the time domain by using Eq. (2.51). Figure 2.5 shows experimental data of the electric modulus at different temperatures for several ionic conductors. Since the plot is in a double logarithmic scale, the linear behavior at both sides of the peaks is indicative of the power law frequency dependence of the complex conductivity. Modulus plots are usually presented in a linear scale, showing asymmetric peaks for the imaginary part ($M''(\omega)$) shifting to lower frequencies when temperature is decreased. However, the linear scale obscures relevant features of the modulus spectra, like, for example, the mentioned power law dependences. The asymmetric power law behavior of the electric modulus data at low and high frequencies, suggests that conductivity relaxation may be described using a Havriliak-Negami (HN) relaxation function

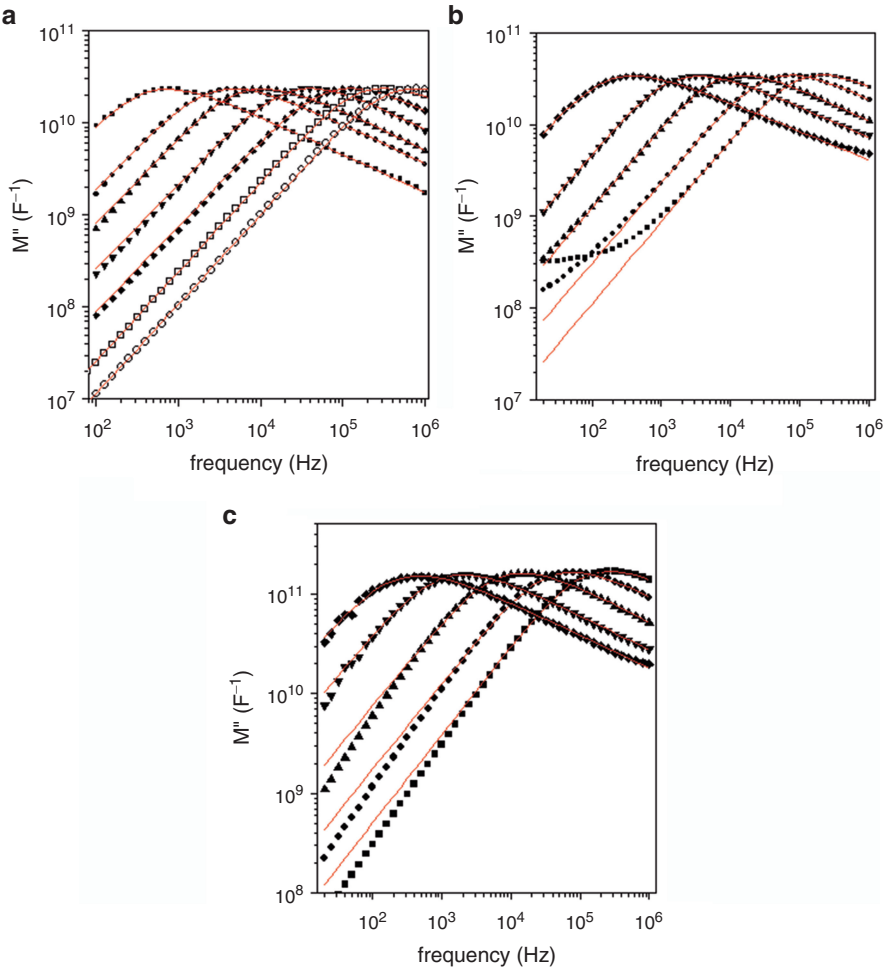

Fig. 2.5 Imaginary part of the dielectric modulus against frequency presented in a double logarithmic scale for (**a**) single-crystal YSZ at 480, 514, 532, 560, 587, 615 and 639 K (from *left to right*), (**b**) $Li_{0.5}La_{0.5}TiO_3$, at 179, 193, 206, 221 and 245 K (from *left to right*) and (**c**) $Li_{0.5}Na_{0.5}La(CrO_4)_3$, at 262, 275, 296, 317 and 336 K (from *left to right*). The *solid curves* are fits to Havriliak-Negami functions according to Eq. (2.53) (see text). Reproduced from [56] with permission

(see Eq. (2.28)), and it is indeed the case as shown by the lines in Fig. 2.5 that are fits of experimental data to a HN function [56].

The discrepancies observed between experimental data of $Li_{0.5}La_{0.5}TiO_3$ and the corresponding fitting functions at low frequencies and high temperatures, are due to blocking effects. Blocking appears as a consequence of charge built ups at grain boundaries or electrodes and do not affect experimental data at high frequencies. This is further discussed in Chap. 4.

The parameters τ_{HN}, α and β in Eq. (2.28) that best fit experimental data can be used to construct an analytical distribution of relaxation times ($\rho(\tau)$) according to the following expressions:

$$\rho(\tau) = \frac{1}{\pi} \frac{(\tau/\tau_{HN})^{\alpha\beta} \sin(\beta\theta)}{\left[(\tau/\tau_{HN})^{2\alpha} + 2(\tau/\tau_{HN})^{\alpha} \cos(\alpha\pi) + 1\right]^{\beta/2}}, \tag{2.52a}$$

where θ is

$$\theta = \arctan\left|\frac{\sin(\alpha\pi)}{(\tau/\tau_{HN})^{\alpha} + \cos(\alpha\pi)}\right|. \tag{2.52b}$$

According to Eq. (2.36) we can relate the dielectric modulus to the Havriliak-Negami function $F^*_{HN}(\omega)$ through :

$$1 - M^*(\omega)/M_\infty = F^*_{HN}(\omega) = -\dot{\Phi}^*(\dot{\omega}). \tag{2.53}$$

And from the distribution of relaxation times obtained from the fitting to a HN function and using Eq. (2.52), the frequency dependence of the Fourier transform of the time derivative of the decay function can be expressed as a superposition of Debye-like processes of the form:

$$-\dot{\Phi}^*(\omega) = \int_0^\infty \frac{\rho(\tau)}{1 + j\omega\tau} d\tau. \tag{2.54}$$

So that in the time domain the following expression holds,

$$\Phi(t) = \int_0^\infty \rho(\tau) e^{-t/\tau} d\tau, \tag{2.55}$$

which allows determining the time decay function from $\rho(\tau)$ by numerical integration. In order to evaluate numerically the integral in Eq. (2.55) it is better to use $\ln\tau$ as integration variable instead of τ, because of the smoother dependence of the integrand on $\ln\tau$. Note also that since the contribution due to small and large values of τ compared to τ_{HN} is negligible, the infinite range of integration do not pose a problem, and it is enough to perform the numerical integration at a finite interval around τ_{HN} to obtain a good approximation to the time decay function $\Phi(t)$.

Finally, once the time decay function Φ(t) has been obtained from experimental electric modulus data using the procedure explained above, it is possible to verify whether or not this function is well approximated by assuming a KWW dependence (see Eq. (2.49)), and eventually obtain the parameters τ^* and n which describes the relaxation process in the time domain. The time decay functions and their fittings to stretched exponential functions with a KWW behavior are presented in Fig. 2.6 at different temperatures for the three systems analyzed. The insets of the figures show

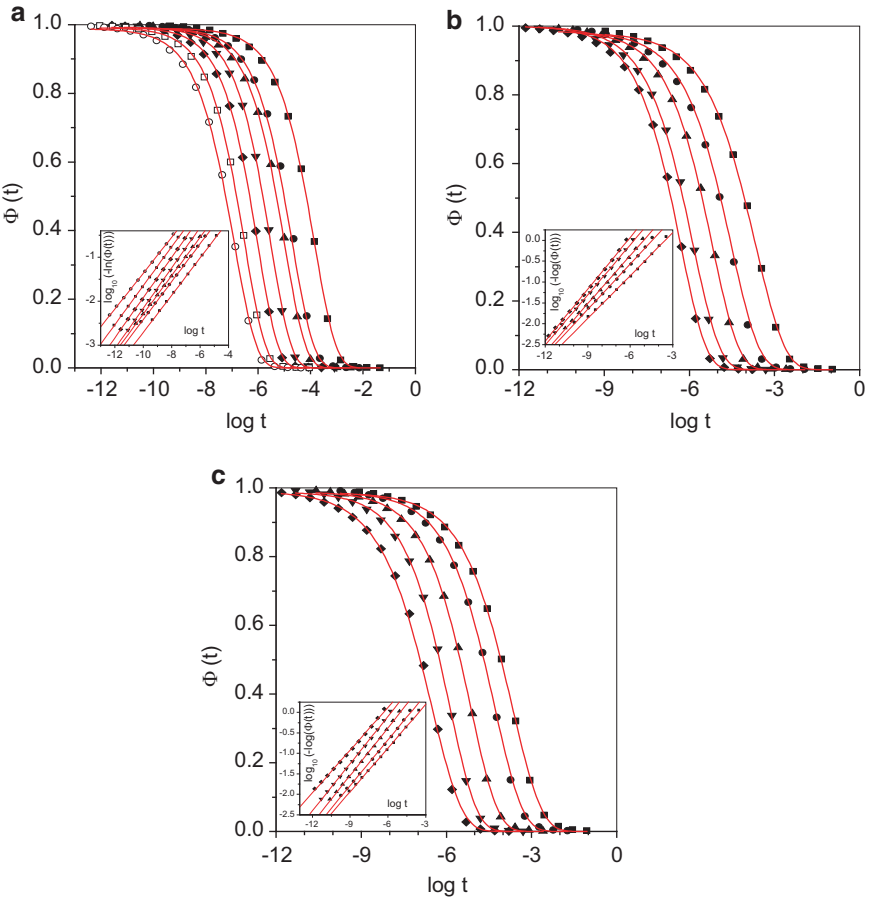

Fig. 2.6 Time decay functions $\Phi(t)$ obtained for (**a**) single-crystal YSZ at 480, 514, 532, 560, 587, 615 and 639 (from *right to left*), (**b**) $Li_{0.5}La_{0.5}TiO_3$, at 179, 193, 206, 221 and 245 K (from *right to left*) and (**c**) $Li_{0.5}Na_{0.5}La(CrO_4)_3$, at 262, 275, 296, 317 and 336 K (from *right to left*). The *solid curves* are fits to KWW functions. The *insets* show log (-ln [$\Phi(t)$]) against log t plots, and the *solid lines* are linear fits. Reproduced from [56] with permission

the corresponding linear log[-ln($\Phi(t)$)] versus log t plots from which parameters τ^* and n were obtained by a linear least-squares fitting.

Although an analytical relationship does not exist between the HN function in the frequency domain and the KWW in the time domain because they are not exactly Fourier transforms of each other, a connection among the parameters of both descriptions has been proposed in the past for dielectric relaxation in polymeric systems [57]. It has been shown that the empirical relation $\alpha\,\beta = (1-n)^{1.23}$ that approximately holds in those systems is also valid naturally in the case of ionic conducting materials, at least for a limited range of values of the parameter n in the KWW function [56]. The relaxation time τ_{HN}, on the other hand, is thermally activated with the same activation energy than τ^* and the dc conductivity.

Once we have obtained the parameters τ^* and n that best fit the conductivity relaxation to a KWW function in the time function, an average relaxation time $\langle\tau\rangle$ can be defined in terms of the integrated area of the KWW function as

$$\langle\tau\rangle = \int_0^\infty \Phi(t)dt = \frac{\Gamma(1/(1-n))}{1-n}\tau^*, \tag{2.56}$$

where Γ refers to the Euler's gamma function [58]. This average relaxation time $\langle\tau\rangle$ is related to the dc conductivity through the following expression:

$$\langle\tau\rangle = \varepsilon_0\varepsilon_\infty/\sigma_0. \tag{2.57}$$

The relaxation time $\langle\tau\rangle$ results to be temperature dependent according to the expression

$$\langle\tau\rangle = \tau_\infty \exp(E/kT) \tag{2.58}$$

so the dc conductivity is also temperature activated and can be expressed as

$$\sigma_0 = \frac{\varepsilon_0\varepsilon_\infty}{\tau_\infty}\exp(-E/kT) \tag{2.59}$$

since the high frequency permittivity $\varepsilon_0\varepsilon_\infty$ usually shows weak temperature dependence. The temperature dependence of the dc conductivity thus obtained is presented in Fig. 2.7 in an Arrhenius plot (open symbols), where the thermally activated behavior results in an apparent linear behavior with slopes determined by the activation energy E. Figure 2.7 also shows the values of the dc conductivity

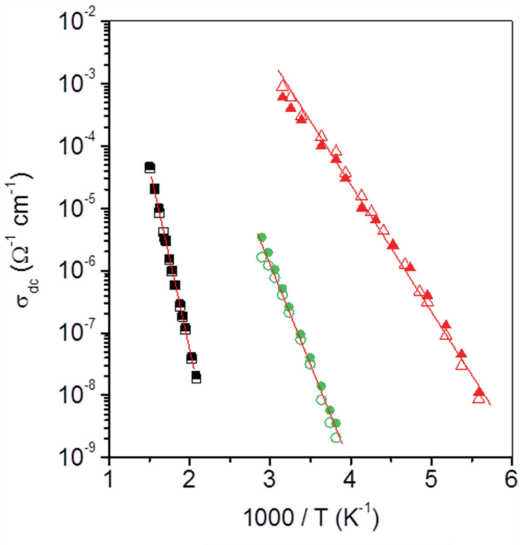

Fig. 2.7 Arrhenius plot of dc conductivities of YSZ (*open squares*), $Li_{0.5}La_{0.5}TiO_3$ (*open triangles*) and $Li_{0.5}Na_{0.5}La$ (CrO4), (*open circles*), obtained assuming a KWW behaviour for the time decay functions. The *solid lines* are fits according to Eq. (2.59). Dc conductivities obtained from complex impedance plots are also displayed as *solid symbols*. Reproduced from [56] with permission

obtained at each temperature from the fitting of the frequency dependent ac conductivity to Eq. (2.47) (solid symbols). A very good agreement can be observed between these results and those deduced from the time decay functions assuming a KWW dependence, which may be considered as an additional evidence for the KWW behavior of the conductivity relaxation in the time domain and the validity of Eq. (2.57).

2.3.4 Ion Diffusion Mechanisms

In crystalline ionic conductors, ion diffusion takes place by the hopping of mobile ions from site to site in the lattice. This explains the temperature dependence of the dc conductivity due to long range ion transport, which, with few exceptions, is found to be thermally activated. The thermal activation results from the energy barrier that ions need to overcome in order to jump to an available neighbouring site in the structure. The existence of different types of structural defects gives rise to several possible diffusion mechanisms for the ions [59]. For example, the diffusion is said to take place by the *vacancy mechanism* if ions jump into an adjacent unoccupied lattice site (vacancy). These vacancies can be point defects, or structural vacancies, that can be created in large amounts for example by doping of CeO_2 or ZrO_2 by substituting Ce and Zr for aliovalent cations as Gd, Sm, Y…, resulting in a large concentration of oxygen vacancies that are responsible of the ionic conductivity in these fluorite structures. Note that vacancies move in the direction opposite the oxide ions. The vacancy mechanism is most often found in fast ionic conductors but there are other different mechanisms that can give rise to high ionic conductivity, like the *interstitial mechanism* that occurs when an ion occupying an interstitial site moves to one of the neighbouring interstitial sites (see Fig. 2.8). In order such a jump to happen between interstitial sites, a large distortion of the lattice is usually required, so its probability is higher the smaller the size of the mobile interstitial ions compare to the ions in lattice sites.

$La_2NiO_{4+\delta}$ is an example of an ionic conductor showing oxide ion diffusion by an interstitial mechanism. In this and other materials with the perovskite related structure of the K_2NiF_4 type, excess oxide ions can be easily accommodated in interstitial sites, giving rise to high oxide ion conductivity. Materials where ion diffusion takes place by interstitial mechanism have the advantage that mobility is not limited by the vacancy-dopant association that usually occurs in materials showing the vacancy mechanism. However, interstitial occupancy usually gives rise to changes in the oxidation state of ions in the lattice and thus to an additional electronic conductivity. In fact, all materials known up to date showing ion conductivity by interstitial mechanism are not pure ionic conductors but they show also electronic conductivity.

Other mechanisms for ion diffusion in solids have been proposed. In the case that interstitial diffusion would require a lattice distortion too large, this mechanism becomes improbable and interstitial ions may move by pushing one of its nearest

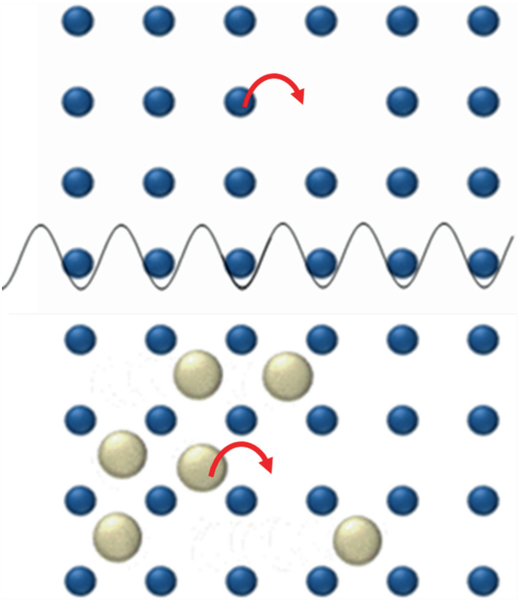

Fig. 2.8 (*Top*) Sketch of the vacancy mechanism for ion diffusion, where the diffusion takes place if ions are able to jump into adjacent unoccupied lattice sites (vacancies). The *line* represents the potential energy barrier that ions must overcome in order to jump. (*Bottom*) Sketch of the interstitial mechanism for ion diffusion, where an ion occupying an interstitial site moves to one of the neighbouring interstitial sites. A large distortion of the lattice is usually required in order such a jump to happen between interstitial sites

neighbours on a lattice site into another interstitial position and itself occupies the lattice site of the displaced atom. This is known as the *interstitialcy mechanism*. Note that it is necessary for an ion to move that there is an interstitial atom on a neighbouring site, and consequently the diffusion coefficient is proportional to the concentration of interstitial ions. A variation of the interstitialcy mechanism is the so called crowdion, where an ion is assumed to be crowded into a line of other ions, causing them to move along the line from their equilibrium sites.

In the last years, the combination of experimental data and computer modelling techniques have led to deeper understanding of the relationships between ion transport mechanisms and the local structure and defect types of ionically conducting materials, allowing materials optimisation for specific applications [60–63].

For the special case of proton diffusion in solids, two different mechanisms have been proposed: the free transport mechanism and the vehicle mechanism. The free transport, also known as Grotthuss mechanism, is usually the way protons diffuse in oxides. For a review see Ref. [64]. The protons jump from one oxygen ion to a neighbouring one, and after each jump the proton in the hydroxide rotates such that the proton reorients in the electron cloud and becomes aligned for the next jump. The rotation and reorientation may involve small activation energy, but it is

believed that the jump itself accounts for most of the activation energy required in the diffusion process. In the vehicle mechanism the proton moves as a passenger on an oxide ion, and thus it actually consists of transport of hydroxide ions. These hydroxide ions may diffuse by an oxygen vacancy mechanism or as an interstitial hydroxide ion. It is worthwhile to remark that the hydroxide ion has a smaller radius and charge than the oxide ion and it is thus expected to have smaller activation energy for diffusion than the oxide ion. Other species such as hydronium ions, H_3O^+, or water molecules may serve as vehicles for proton diffusion, particularly in open structures [59, 65].

The mechanisms described above are for ion diffusion in crystals. But microstructure in crystals can play a major role in ion diffusion. For example, lower activation energy for ion diffusion is often found along certain dislocations and along the grain boundaries in polycrystalline materials compare to bulk values. In general, surface diffusion occurs much faster than grain boundary diffusion, and grain boundary diffusion occurs much faster than lattice diffusion. Thus, in polycrystalline materials an effective diffusion coefficient is introduced which is a combination of the diffusion coefficients along the different regions. This is particularly relevant in the case of nanocrystalline materials, where the grain boundaries may be a significant fraction of the material, and thus result in an enhancement of ion diffusion (see Chap. 5). Finally, amorphous, glassy or liquid ionic conductors are often described as disordered lattices with a landscape of energy barriers for ion hopping, and where pathways for enhanced ion transport may exist compared to the crystalline structure with same chemical composition.

2.3.5 Temperature Dependence of Ion Diffusion

Independently of which is the mechanism involved in ion diffusion through the material, the mobile ions have to overcome a potential (energy) barrier of height ΔH_m in order to jump from site to site in the structure. This is schematically shown in Fig. 2.9. At a given temperature, ions are vibrating within their cages and have a finite probability of jumping outside the cage which is proportional to $\exp(-\Delta H_m/k_BT)$. The diffusion will be thermally activated and the energy barrier ΔH_m represents the activation energy for ion hopping. If one considers the equilibrium state for the ion, the energy minimum and its activated state at the maximum energy between equilibrium sites, it can be shown that the transition rate between equilibrium sites is given by [66]:

$$\Gamma = \nu_0 e^{-\Delta G_m/k_BT} = \nu_0 e^{-\Delta S_m/k_B} e^{-\Delta H_m/k_BT} \tag{2.60}$$

where ν_0 represents the vibration or "attempt" frequency of the mobile ion within the potential cage, of the order of $\nu_0 \sim 10^{13}$ Hz, and ΔG_m, ΔS_m, and ΔH_m represent the Gibbs free energy, entropy and enthalpy change respectively, characterizing the

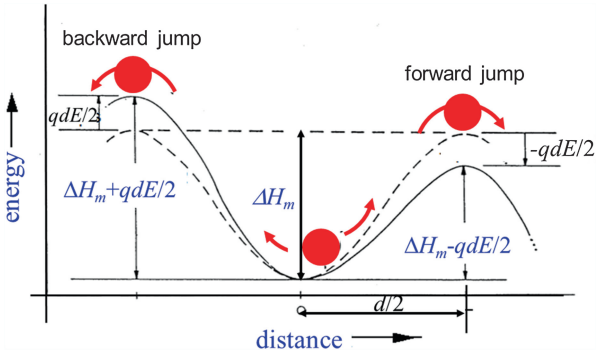

Fig. 2.9 One dimensional model for jump diffusion in an ionic conductor. In the absence of an applied electric field, the probability of the ion of jumping in either forward or backward direction is the same. The activation energy for ion hopping is always ΔH_m and the transition rate (jump frequency) for forward and backward jumps will be the same. When an electric field of magnitude E is applied, the jump frequency in the forward direction is increased, while the jump frequency in the backward direction is decreased. Figure adapted from reference [59]

ion displacement from its equilibrium state to its activated state at the top of the potential barrier. Assuming the vibration of the ion can be described as a harmonic oscillator, the attempt frequency can be estimated to be of the order of $\nu_0 \sim \left(\sqrt{\Delta H_m/M}\right)/x_0$, with x_0 the jump distance and M the reduced mass of the oscillator. Therefore, it is expected that the smaller the value of the enthalpy change ΔH_m, the lower the value of the preexponential factor in the diffusion coefficient in Eq. (2.42–2.45). This behaviour gives rise to a compensation effect that is in fact observed in experimental data and that it is known as the Meyer-Neldel rule. However, it is often found experimentally that a decrease in ΔH_m results in a value of the preexponential factor much lower than predicted by this simple effect of the Meyer-Neldel rule [67].

Another factor determining the temperature dependence of the diffusion coefficient is the concentration of available sites where the mobile ions can jump to. However, for the sake of simplicity we will consider here that this concentration is temperature independent, which is often the case for fast ionic conductors in the experimental temperature range of interest.

2.3.6 *One Dimensional Random-Hopping Model for Ionic Conductivity*

Figure 2.9 illustrates a simple one dimensional model for jump diffusion in an ionic conductor [59]. In the absence of an applied electric field, the probability of the ion of jumping in either forward or backward direction is the same. The activation energy for ion hopping is always ΔH_m and the transition rate (jump frequency) for

forward and backward jumps will be the same. Therefore, in a given time interval, the number of jumps in both directions will be the same. If the material is homogeneous, we can conclude that there will be no net transport of ions in the material. When an electric field of magnitude E is applied, the jump frequency in the forward direction is increased since the activation energy is decreased by an energy $qdE/2$ (see Fig. 2.9),

$$\Gamma_f = \nu_0 e^{\frac{\Delta S_m}{k_B}} e^{-\left(\frac{\Delta H_m - qdE/2}{k_B T}\right)}, \tag{2.61a}$$

with q the electric charge of the hopping ion and $d = x_0$ the jump distance. Similarly the jump frequency is decreased in the backward or reverse direction since the activation energy is increased by an energy $qdE/2$,

$$\Gamma_r = \nu_0 e^{\frac{\Delta S_m}{k_B}} e^{-\left(\frac{\Delta H_m + qdE/2}{k_B T}\right)}. \tag{2.61b}$$

We can calculate the current density from the difference of the forward and reverse directions,

$$j = \tfrac{1}{2} nqd\left(\Gamma_f - \Gamma_r\right), \tag{2.62a}$$

where n is the concentration of hopping ions. Therefore, by using Eq. (2.61) we can write

$$j = \tfrac{1}{2}\, nqd\,\nu_0 \exp\left(\frac{\Delta S_m}{k_B}\right)\exp\left(\frac{-\Delta H_m}{k_B T}\right)\left[\exp\left(\frac{qdE}{2k_B T}\right) - \exp\left(\frac{-qdE}{2k_B T}\right)\right]. \tag{2.62b}$$

If, as it is usually the case, the electrostatic term is much lower than the thermal energy of the ion, $qdE << k_B T$, we can use the approximation $e^x - e^{-x} \approx 2x$ for $x << 1$, and get

$$j = \tfrac{1}{2} nqd\,\nu_0 \exp\left(\frac{\Delta S_m}{k_B}\right)\exp\left(\frac{-\Delta H_m}{k_B T}\right)\frac{qdE}{kT}. \tag{2.63a}$$

$$j = \frac{nq^2 d^2 \Gamma}{2kT} E. \tag{2.63b}$$

The factor 1/2 in our one dimensional model becomes 1/6 for a three dimensional diffusion in a cubic structure.

$$j = \frac{nq^2 d^2 \Gamma}{ZkT} E = \frac{nq^2 d^2 \Gamma}{6kT} E. \tag{2.63c}$$

The factor Z may be different in materials with other structures where ion diffusion is favoured in some particular directions.

The expressions for the electrical conductivity and for the diffusion coefficient in a 3D cubic structure are finally given by

$$\sigma_0 = \frac{nq^2 d^2 \Gamma}{6kT} = \frac{nq^2 D_0}{kT}, \tag{2.64a}$$

$$D_0 = \frac{d^2 \Gamma}{6}. \tag{2.64b}$$

Note that this simple random-hopping model for ion diffusion results in the Nernst-Einstein equation introduced above (see Eq. (2.42–2.45)), and it also explains the thermally activated behaviour of the diffusion coefficient in ionic conductors.

Before ending this section, we discuss the case when the electric field that the ions feel is so large that the approximation $qdE << k_B T$ does not hold. At room temperature, for ions with charge $q = \pm e$, and for typical jump distances of a few angstroms, it involves that the electric field must be larger than $\sim 10^8$ V/m which is extremely high. In fact, the opposite condition $qdE >> k_B T$ can sometimes be fulfilled, and Eq. (2.63) can then be approximated by

$$j = \tfrac{1}{2} nqd\nu_0 \exp\left(\frac{\Delta S_m}{k_B}\right) \exp\left(\frac{-(\Delta H_m - qdE/2)}{k_B T}\right). \tag{2.65}$$

These large electric fields, of the order of $\sim 10^8$ V/m or larger, may easily exist in nanostructured materials (see Chap. 5). If a voltage difference of just a few volts is applied for example to a thin film of an ionic conducting material with a thickness of just a few nanometers, the term $qdE/2$ can be as large as hundreds of millielectron-volts and then, not only it is larger than the thermal energy, but even comparable to ΔH_m in Eq. (2.65). In this case, non-linear ion diffusion occurs, even at low temperatures, since the effective activation energy can be very small under the application of such large electric fields.

2.4 Non-Gaussianity of Dynamics

The intermediate scattering function, $F_s(k,t)$, obtained by neutron scattering and/or molecular dynamics simulations (see Sect. 8.3.3.2) also shows stretched exponential decay and this is known to be a common character of the slow dynamics observed in many glass forming materials. The functional form is closely related to the Non-Gaussianity of the diffusive motion. In this subsection the relationship between non-Debye relaxation and non-Gaussianity of the dynamics in the real space is discussed.

The intermediate scattering function, $F_s(k,t)$ is connected to the self-part of the van Hove function (see Sect. 8.3.3.1) by the Fourier transform [68]

$$F_s(k,t) = \int 4\pi r^2 G_s(\mathbf{r},t)\frac{\sin(\mathbf{k}\bullet\mathbf{r})}{\mathbf{k}\bullet\mathbf{r}}dr. \tag{2.66}$$

When the van Hove function spreads to a distance r_c, the mean squared displacement (MSD) $<r_i(t)^2>$ is represented by

$$<r_i(t)^2>=\int_0^{r_c} r^2 \bullet 4\pi r^2 G_s(r,t)dr \tag{2.67}$$

Therefore, the functional form of the stretched exponential is connected how the mean squared displacement of particle changes with an elapse of time (see Sects. 9.4 and 11.3).

The function $F_s(k,t)$ can be approximated by the following equations [69].

$$F_s(k,t) \approx exp\left[-\frac{k^2}{2d}<r_i^2(t)>+\frac{k^4}{2}\left(\frac{r_i^2(t)}{2d}\right)^2\alpha_2(t)\right], \tag{2.68}$$

where α_2 is the non-Gaussian parameter and d is the spatial dimension. The value α_2 becomes 0, when the Dynamics has a Gaussian form and therefore, the parameter represent the deviation from the Gaussian form. On the other hand, k^2 dependence of the $F_s(k,t)$ mean the Debye type decay of the function. Therefore, Non-Debye functional form is closely related to the non-Gaussianity of the dynamics in the real space. That is, to examine the origin of the power law dependence found in MSD is equivalent to examine the origin of stretched exponential decay.

Non-Gaussianity of the dynamics is thus observed by using deviation from the Gaussian function of self-part of the van-Hove functions, wave number dependence of $F_s(k,t)$, and non-Gaussian parameters. In the self-part of the van Hove function, obviously the tail part with inverse-power law (with exponential truncation) exists and it means the existence of the longer length scale of the motion, related to the Lévy distribution of wider sense [see A.2.2]. This feature is commonly appeared in ionic systems and in other glass forming materials. Therefore, the motion of particles has the distribution of distances, which is different from the Gaussian dynamics. Thus the non-Gaussianity is also a signature of the cooperative dynamics.

2.4.1 Relation Between Jump Rate and Relaxation Rate in the Stretched Exponential Decay: From the Modeling by the Molecular Dynamics Simulations

It is noteworthy to mention that the time scale of the elementary ion jump motion is not the same as that of the diffusive motion as will be shown in the several characteristic time regions in the mean square displacement (MSD) of ions in glassy ionic conductors (see Sects. 9.4.1, 9.4.4 and 11.3). For example, the first

successful jump motion of ion at 700 K of the lithium metasilicate (Li_2SiO_3) system in the glassy state is found at around 10–20 ps region, while the diffusive region starts at around 500 ps. This situation is made clear in this subsection by the result of MD simulations. It also means that the activation energy of each jump motion is different from those for diffusive and/or conduction. Similar discussion also holds for several relaxation functions such as $F_s(k,t)$. Namely, the distribution of jump rates is different from the relaxation rate of the stretched exponential functions. Waiting time distribution assumed in some theories are also observed in the MD simulations of ionic systems, and this distribution partially explain the various events found at the different time scales. However, the difference of time scales is coming from not only by the wide distribution of jump rates but also by the geometrical correlation among successive jumps, where both the back and forward correlated motions of ions contribute.

Frequency dependent behavior of the conductivity [see Sect. 8.3.2.2] can also be connected to the MSD in the real space by the following relation [70, 71]:

$$\sigma^*(\omega) = -\omega^2 \frac{Nq^2}{6H_R kT} \int_0^\infty < r^2(t) > e^{-i\omega t} dt, \tag{2.69}$$

where N is the number density of mobile ions, q the ion charge, k the Boltzmann constant, H_R the Haven ratio and T the temperature.

Each of the variety of ionic motions is not simple as shown in the following examples. In Fig. 2.10, examples of two dimensional projections of trajectories of one Li ion observed by MD for glassy Li_2SiO_3 at 700 K during 500 ps run (This time scale corresponds to the beginning of the diffusive regime ($=t_{dif}$, see Sect. 9.4.2)) are shown for three cases. In the upper panel, trajectory is projected on XY plane, while in the lower panel, it is projected on YZ plane. Several kinds of jump motions are found in MD of ionic systems including strong localized motion within the neighboring sites and forward correlated jumps which are highly cooperative.

In Fig. 2.11 a three dimensional plot of the same trajectories is shown. The complexity of the motion is clear when you compared it with the simple three dimensional random walk shown in the lower panel. The dense part of the trajectory means that the ion is caged by the surrounding particles for a long time at the so called ion site. This situation is consistent with the existence of clear peaks in the pair correlation functions, $g(r)$ for Li-Li pair. The site represented by the localization of the trajectory shows a variety in size, shape and density, indicating the existence of multifractality. One can see the both long ranged motion and localized motion, and the mixing of them.

During this period, some ions tend to be localized for long times, while some other ions continued many back correlated jumps and a limited number of ions tends to show an accelerated dynamics and such motions are accompanied of cooperative jumps of several ions. Among these different type of motions, contribution of the fast (accelerated) ions to MSD is large, because the displacement is

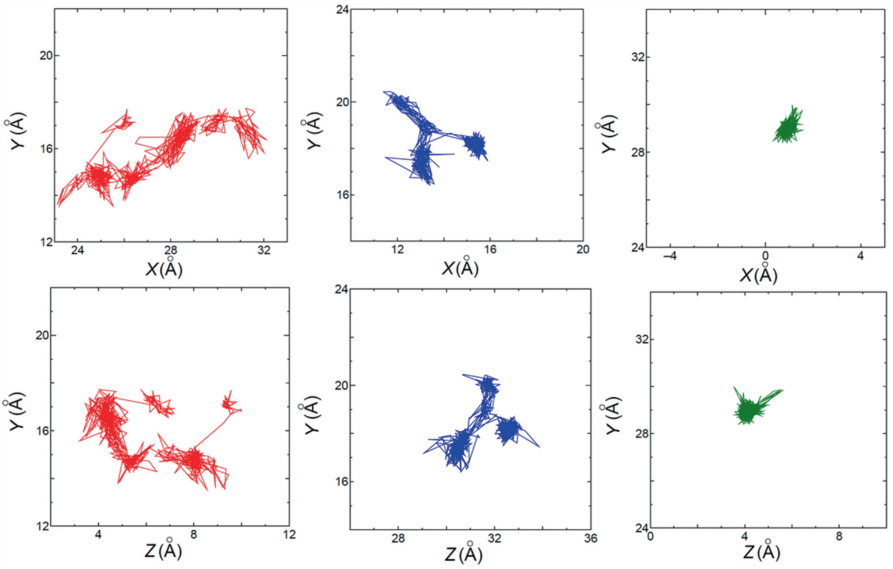

Fig. 2.10 Examples of trajectory of Li^+ ion in Li_2SiO_3 system at 700 K during 500 ps obtained by MD simulations. This time scale corresponds to the beginning of the diffusive regime, t_{dif}. *Upper panel* is for XY projections and *lower panel* is for ZY projections. In the *left panel* (*red curves*), starting position of the motion is (X = 29.8, Y = 17.4, Z = 6.2), while ending position is (X = 26.2, Y = 17.2, Z = 9.3) (in Å). In the *middle panel* (*blue curves*), starting position of the motion is (X = 13.2, Y = 17.0, Z = 30.4), while ending position is (X = 15.4, Y = 18.3, Z = 32.6) (in Å). In the *right panel* (*green curves*) starting position of the motion is (X = 1.1, Y = 28.4, Z = 4.0), while ending position is (X = 1.1, Y = 29.1, Z = 4.2) (in Å). Squared displacement, r_i^2 at the end positions of *left*, *middle*, and *right* examples are, 23.7, 11.0 and 0.5 $Å^2$, respectively. The contribution of accelerated dynamics is large. The dynamics are extremely heterogeneous. Accelerated jumps, localized jumps and long time localization and mixing of such motions are found as discussed in Chaps. 9 and 11. That is, the time scale of the power law dependence of MSD (or stretched exponential decay) is not for a single jump process. Note that the motions are just examples. Note that if the observation time was short, only localized motion might be found

squared in calculation of it. An example of cooperative motions is shown in Fig. 2.12. The ion tends to show further successive jumps.

Similar situation is also found for the system with lower diffusivity. Another example for the motions of Li ions and atoms for a slice of MD cell in lithium disilicate ($Li_2Si_2O_5$) glass at lower temperature of 600 K for longer scale 8 ns runs is shown in Fig. 2.13. Heterogeneous dynamics of Li ions and partial formation of ion channels, which are formed dynamically by cooperative jumps along the networks formed by SiO_4 units, are observed. For the calculation of mean square displacement (MSD), one needs to use many numbers of ions and many initial times to average it [see Sect. 8.5].

Thus ionic motion of ions itself is highly heterogeneous and one needs to consider effect of heterogeneity caused by cooperativity of motions. We will discuss the characteristics of several theories and models here with the aid of MD

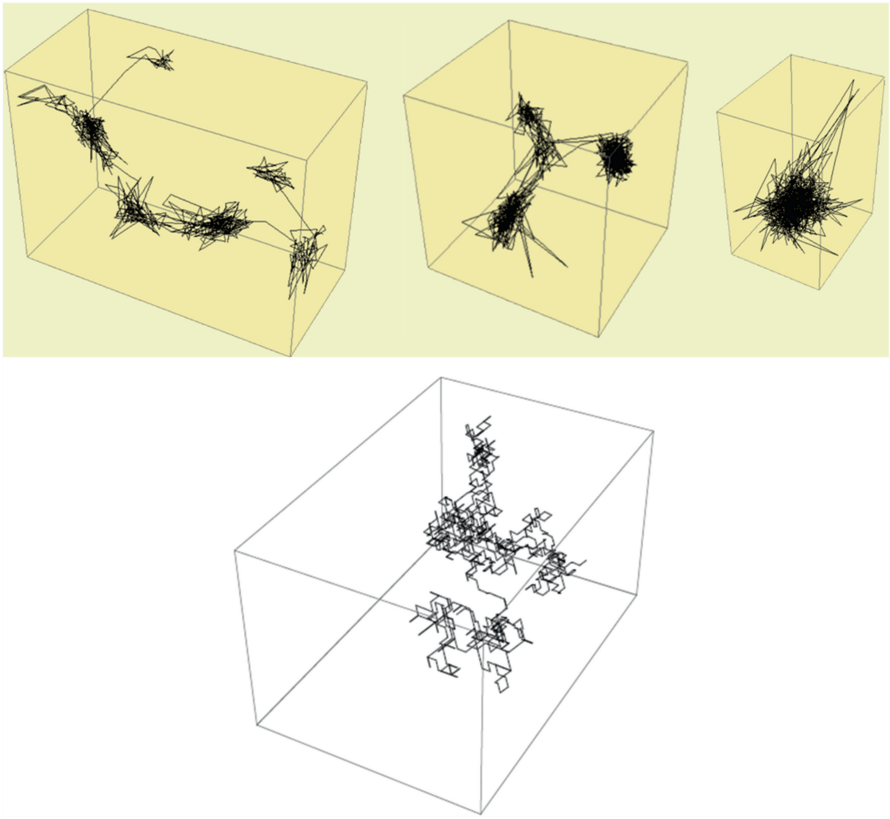

Fig. 2.11 (*Upper panel*) Three dimensional plot of the trajectories of Li ions shown in Fig. 2.10. Ionic motion is a complex one with mixing of strong back correlated motions, waiting time distribution and existence of accelerated motion. (*Lower panel*) Three dimensional plot of an example of 3D random walk (1000 steps). One can see the ionic motion in the glassy state is quite different from the random walk

simulations. These complex behaviors of ions can be well characterized by considering the fractal nature of the motion represented by both temporal (related to the distributions of jump rate or waiting time) and spatial terms (related to the correlation among successive motions and distribution of length scale).

2.4.2 Relation Between Power Law Exponent of MSD and Characteristics of Jump Motions

In this subsection, we consider the cause of power law behavior of MSD based on the characteristics of jump motions. As already shown in Sect. 2.3.4, non-Debye character of the relaxation of the ionic motion are often explained by the temporal

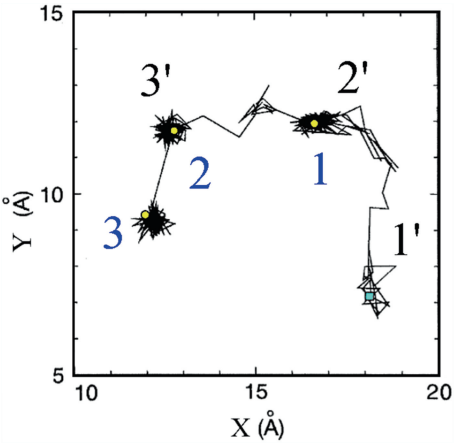

Fig. 2.12 Example of cooperative jumps of Li ions in the Li_2SiO_3 glass at 700 K projected on X-Y plane. Initial positions of three Li ions are 1, 2 and 3 (marked by *yellow circles*), while the last position of the ions after 16 ps run is 1', 2' and 3'. The last position of the first ion is marked by a *pale blue square*. The first ion shows a long jump (~twice of the typical distance among ion sites) without a clear trapping. The second ion is found to be located between two sites for a while, until the vacant site is available. Thus availability of the vacancy is closely related to the cooperative jumps

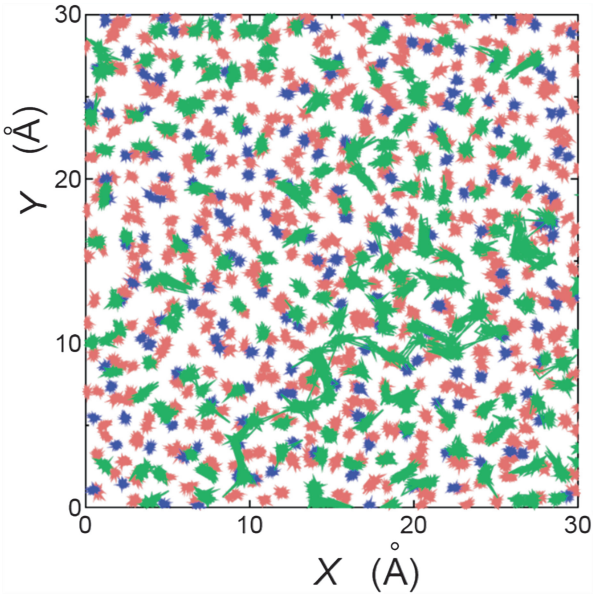

Fig. 2.13 Trajectories of ions and atoms represented for 10 Å in a slice in thickness of MD cell for Lithium disilicate at 600 K, during 8 ns run. *Green*: Li ions, *Blue*: Si atoms, *Red*: O atoms. Motion of Si and O atoms are essentially localized. The dynamics of Li ions is heterogeneous. Formation of a part of the ion channels is observed, while many ions are showing localized motions. In this case, t_{dif} is longer than 15 ns

and/or spatial terms of jump motions and therefore, this is also related to the non-Gaussian character of the diffusive dynamics. In real space, the relation between jump motions and behavior of the MSD is connected by the theory of fractal and/or percolations, and the power law dependence of MSD is argued to be related to the fractal dimension of walks or jumps and their paths contributing to the MSD. Therefore the concept of fractal [72] is useful to consider the relationship between characteristics of jump motions and the functional forms of the MSD. In the following, we discuss the approaches that are related to the characteristics of jump motions in ionic system and related materials. (See Sect. 2.3.4 for related mechanisms suggested for crystals and see also Sect. 9.10 for the comparison of crystal and glass by MD simulations.)

Elliott has discussed [73] the two possible mechanisms of the AC conduction, which corresponds to the power law behavior of MSD (see Sect. 9.4.2) of ions. In the parallel conduction, ion jumps independently with the distribution of the relaxation rate, while in the series conduction, the site causes a relaxation coupled with other sites.

AC hopping conductivity of the one dimensional bond percolation was discussed by Odagaki and Lax [74] based on the distribution of the random interruptions. Odagaki [75] also discussed the stochastic trapping transport assuming the waiting time distribution of jump motions with the use of the generalized coherent medium approximation.

Strong localization in the solid state can be also explained by the fractal dimension of the motion and paths. Alexander and Orbach discussed the vibrational excitation by "fracton" [see Appendix A.2.1 for details], determined by fractal dimension of walks and that of their paths. The mode is discussed as an origin of the "boson peak" [76], which is one of the characteristics commonly found in glasses. On the basis of the relaxation mode theory, Ishii [77] has discussed the hopping on the fractal lattice and found the "fracton" of the hopping version. The approach was expanded to the many particle problem of weak coupling case [78] and the appearance of the both diffusive and non-diffusive mode was discussed.

Bunde et al. [79] have examined the localized excitation on the incipient infinite percolation cluster and discussed the relation to the multifractality.

2.4.3 Relation Between the Theory of Fractal and the Characteristics of Jumps

These theories mentioned in the above explain well some parts of findings by experiments and/or simulations. However, the mechanisms assumed therein are not necessarily the same. Here we introduce some fractal dimensions (exponents) to characterize the dynamics of ions by the fractal nature of the jump motions, where waiting time distribution, distribution of length scale, fractal dimensions of paths and/or their combinations are taken into account. Then we consider how we can distinguish these contributions by MD simulations.

Readers may not be familiar with technical terms such as fractal, fracton, multifractal, Lévy flight and Lévy distribution (and its truncation) used in the following subsections. Details of such terms are explained separately in the Appendix. By using the CDF files included in ESM, the readers also can manipulate the parameters of Lévy distribution and examine the example of the analysis of such motions. [See Sect. 12.2 for the explanation of Example 2 in ESM.]

If one fractal dimension governs the system, the exponent of the power law behavior of the MSD, θ is connected to the fractal dimension of the random walks, d_w, as a first approximation [72] by,

$$\left\langle r^2(t)\right\rangle \sim t^{\theta}, \;\; \theta = 2/d_w \tag{2.70}$$

For regular diffusion, $d_w = 2$ is expected. However, if the dynamics are beyond random walks, d_w does not equal 2. Specifically, if the motions of the ions involve localized motions, the trajectory becomes more complex and the exponent θ becomes smaller. On the contrary, when ion shows forward correlated jumps with the trajectory becoming linear like, this resulted in the decrease of d_w and increase of θ. The former situation retards the time scale for the start the diffusive regime, while the latter situation causes an opposite case. The exponent d_w of the trajectory of ions can be determined by MD simulations [see Sects. 9.5.4, 11.5.2 and Appendix A.1 for more details] and this can be a direct measure of the power law behavior in MSD of the ionic motion. Although the relation between the complexity of the trajectory and the power law exponent is clear from Eq. (2.70), result of MD simulations reveals that the motion is extremely heterogeneous and not monofractal. In the case of coexistence of fast and slow ions, two length scale regions are found in MD. Therefore, the expansion of the situation to the multifractal walks [80], where two length scales are concerned, is necessary. The large scale motion is found to be caused by cooperative jumps of several ions and successive motions. Therefore, even for the single particle motion, the dynamic heterogeneity affects the exponent connecting different time scale motions. In the collective mode such as conductivity, this relation is further modified by the Haven ratio as shown in Eq. (2.69).

2.4.4 Distribution of Length Scales and Lévy Distribution

Another factor related to the jump motions is concerned with the distribution of the length scales. Lévy distribution and related Lévy flight dynamics is experimentally known to exist in several physical phenomena such as turbulent [81] and Josephson junction [82]. By MD simulation of lithium silicates and in an ionic liquid, we have found that in the power law region of MSD, the dynamics is well represented by the Lévy distribution [83] or Lévy flight [84] (with a Lévy index $\alpha < 2$) related to this distribution, as shown in the inverse-power law tail of the self-part of the van Hove

functions. (See Sects. 9.5, 11.2, 11.5.3 and 11.12.2, see also files in ESM and 12.2 for examples of motions and manipulation of parameters of distributions. See also Appendix A.2–A.4)

2.4.5 Heterogeneity and Multifractal Mixing of Different Length Scales

The observed Lévy distribution by MD is accompanied with an exponential truncation and strong back-correlated motion, and occurrence of the infinite variance of the distribution is avoided by these mechanisms. The Lévy distribution combined with the exponential truncation [see Sect. 11.5.3] shows a multifractal character in a long time region. This view is consistent to the existence of multifractal density profile of ions (see Appendix A.3) formed by such motions.

2.4.6 Separation of Exponents Having Different Origins

As observed in the trajectories of Li ions obtained by MD, both temporal (waiting time distribution) and spatial character (distribution of length scale and back and forward correlated motions) contribute to the dynamics. When the exponent α concerned with distribution of length scale and the exponent γ characterizing the waiting time distribution are coexisting, the relevant question is how the dynamics are modified.

Blumen and coworkers [85] considered the situation where the both temporal and spatial terms contribute to the diffusive motion and obtained the following relation.

$$D(t) \sim d\left\langle r^2(t)\right\rangle/dt \sim t^{\alpha\gamma-1}, 0 < \alpha\gamma < 1 \tag{2.71}$$

Similar argument holds for the exponent of the stretched exponential relaxations. They pointed out that the combination of the exponents giving the same behaviors of the stretched exponential (and time dependence of MSD) is infinitive and it is difficult to separate them if it is overlapped in the time region. They also suggested that the separation of temporal and spatial terms might be possible when the long time behavior is governed by the temporal term. However, this condition of the long time might be difficult to fulfill and to judge within the limited time scale of the observation in the case of MD simulations.

Habasaki and coworkers [86] tried to distinguish temporal and spatial contribution of the dynamics using MD simulations (see Sect. 9.5 for more details, where the same analysis was done with better statistics) by another method. That is, MSD is separated into two plots. In the first plot, the accumulated jump numbers is plotted

against time and in the second plot, MSD was plotted against the accumulated number of jumps. By this analysis, it was clarified that the cause of the power law dependence of MSD is due to the spatial term (geometrical correlation among successive jumps), although waiting time distribution exists and contribute to the slow dynamics through a mean jump rate. (See Sect. 9.5.5 for different view for the contribution of the temporal and spatial terms and cause of the difference.) Even for the motion of a tracer ion (single particle motion), the geometrical correlation found there is affected one by the cooperative motions of surrounding ions (collective motions).

This kind of analysis is useful to clarify the effect of interactions among ions at the same time. This is because, if there was no interaction with surrounding particles, we can expect only the random single jumps. Of course, direct analysis of cooperative motions is also informative as well as fractal dimension analysis of the trajectories.

The method used to separate the terms is applicable to other systems and will be useful to understand the role of temporal and spatial factors. As shown in the present section, the short time behavior of the system is connected by the exponent (fractal dimension) to the long time behavior. We note that this connection is represented well by the Coupling Model by one of the authors, but is not necessarily clearly included in other theories or models. For further details of heterogeneous dynamics observed by MD, see Chaps. 9–11.

2.5 Models of Ion Dynamics

In the following we present a brief discussion of some of the more relevant theoretical models of ion dynamics. Among all the existing models proposed in the literature we have tried to choose those most highly cited. In Chap. 4 we present a further discussion of the models where we have tried to bring out, when possible, their relations with experimental data as well as the extent of their predictions and applications, in order to emphasize the relevant ideas behind the models and also their possible deficiencies. This is relevant since, as Karl Popper said [87], any theory can claim it is correct by choosing its own list of experiments to verify.

2.5.1 Random Barrier Model

As in the simple one dimensional model sketched in Fig. 2.9, other hopping models [88–91] are defined by specifying the allowed transitions and their transition rates for the hopping particles (ions in the case considered here). In order to simplify the models it is usually assumed that the allowed sites for the ions define a regular lattice and that interactions among ions can be neglected, so that it is enough to

consider the motion of just one ion. The random barrier model starts by assuming the particles can take positions only on a simple cubic lattice in d dimensions. The basic quantity characterizing such an ensemble of particles is the probability P_s to be at site $\boldsymbol{s}$. If $\Gamma(\boldsymbol{s} \to \boldsymbol{s}')$ is the probability per unit time for jumps from site $\boldsymbol{s}$ to site $\boldsymbol{s}'$, the "equation of motion" is the well known master equation [90, 92]

$$\frac{dP_s}{dt} = \sum_{s'} [\Gamma(\boldsymbol{s}' \to \boldsymbol{s}) P_{s'} - \Gamma(\boldsymbol{s} \to \boldsymbol{s}') P_s]. \tag{2.72}$$

Equation (2.72) determines the equilibrium dynamics, and from equilibrium fluctuations the velocity autocorrelation function may be calculated where v is the projection of the velocity in a fixed direction. This quantity determines the frequency dependence of the diffusion coefficient $D^*(\omega)$ and the electrical conductivity $\sigma^*(\omega)$ (see Eqs. (2.41–2.42)). In the following, for simplicity of the expressions derived from the model, a unit system is chosen so that $\sigma^*(\omega) = D^*(\omega)$ and where moreover both quantities are normalized such that on a lattice with uniform jump frequency Γ one has $\sigma^*(\omega) = D^*(\omega) = \Gamma$ (note that for a uniform jump frequency the conductivity is frequency independent and given by Eq. (2.64)). It is also useful to define a dimensionless frequency-dependent conductivity by $\widetilde{\sigma^*}(\omega) = \sigma^*(\omega)/\sigma(0)$.

The **random barrier model** (RBM) is defined by a special case of Eq. (2.72) where all sites have equal energy [93]. Figure 2.14 illustrates the random energy landscape of this microscopic model in one dimension. Whenever site energies are equal, by the principle of detailed balance (a consequence of time-reversal invariance) the jump rates are symmetric, i.e. $\Gamma(\boldsymbol{s}' \to \boldsymbol{s}) = \Gamma(\boldsymbol{s} \to \boldsymbol{s}')$. This is why the random barrier model is also referred to as symmetric hopping model. It is assumed that, if the energy barrier height is E, the jump rates are given by the attempt frequency times $e^{-\beta E}$ $\left(\Gamma = \nu_0 e^{-\beta E}\right)$, with $\beta = 1/k_B T$. The model is then completely defined in terms of the energy barrier probability distribution, $p(E)$. In the so called

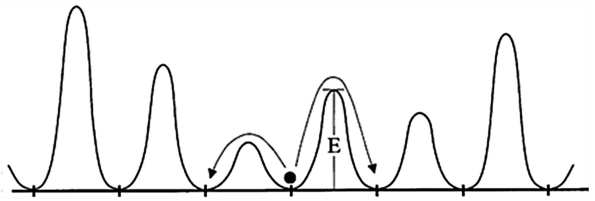

Fig. 2.14 Sketch of a typical potential for a system described by the random barrier model in one dimension. The *arrows* indicate the two possible jumps for the charge carrier shown. At low temperatures most time is spent close to energy minima but, occasionally, a charge carrier by chance acquires enough energy from the surrounding heat bath to jump into a neighboring site. If the barrier height is E, the probability per unit time for a jump is given by $\Gamma = \nu_0 e^{-E/k_B T}$. At low temperatures the charge carrier almost always chooses the lowest barrier. This implies that after one jump the next jump most likely goes back again. Reproduced from [94] with permission

extreme disorder limit, $\beta \rightarrow \infty$, the jump rates vary many orders of magnitude and the random barrier model describes a highly inhomogeneous (heterogeneous) situation.

Because of the broad range of barrier energies that are involved in long range dc transport, a priori one would not expect any particular temperature dependence of the dc conductivity $\sigma_{dc} = \sigma(0)$. However, for strong enough disorder, percolation determines dc conductivity and results in its Arrhenius (thermally activated) temperature dependence [95], which is often observed experimentally. If one considers all the lattice links with barriers below a certain energy, for low energy values, these links form small separated clusters. As the energy value is increased, eventually, for an energy E_c, a fraction of links p_c (the percolation threshold) is reached and an infinite cluster forms, allowing dc conduction. Thus, the activation energy for dc conductivity is the largest barrier on the percolation cluster, E_c, which determines the bottleneck for long range transport and is given by [94].

$$\int_0^{E_c} p(E)dE = p_c. \tag{2.73}$$

The frequency dependence of the ac conductivity can be obtained by solving the master equation in Eq. (2.72) using numerical methods [33]. Figure 2.15 shows computer simulations for different barrier distributions $p(E)$ at large values of the β parameter. These results show that, according to the RBM, the frequency dependence of the ac conductivity is expected to show universal behavior in the extreme disorder limit, i.e. it is independent of the details of the distribution of energy barriers in the material. The best available analytical approximation to this universal ac conductivity response is the diffusion cluster approximation (DCA) [96], which reads

$$ln\tilde{\sigma} = \left(\frac{j\omega}{\tilde{\sigma}}\right)^{d_0/2}, \tag{2.74}$$

where the exponent $d_0 = 1.35$ fits the results from computer simulations of diffusion in three dimensions (see solid line in Fig. 2.15). It is important, however, to note that DCA does not give the same frequency dependence than computer simulations for the imaginary part of the conductivity at low frequencies. Figure 2.15 shows also the prediction of the effective medium approximation (EMA) [33], as given by the expression $ln\tilde{\sigma} = (j\omega/\tilde{\sigma})$, (dashed line), which gives a qualitatively reasonable good fit to computer simulation results, but worse than the diffusion cluster approximation.

The RBM is based on the existence of disorder at a microscopic scale, which seems to be the case for ionic conducting glasses and liquids, although there is no guarantee of whether the disorder is actually relevant for ionic dynamics and conductivity. A macroscopic model has been proposed [33] for systems that are

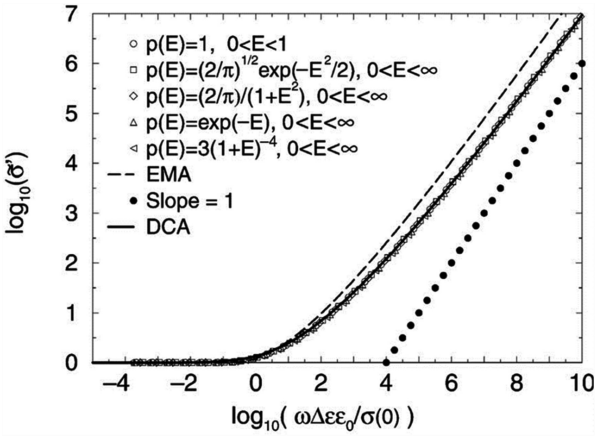

Fig. 2.15 Frequency dependence of the real part of the ac conductivity obtained from computer simulations of the random barrier model for several energy barrier probability distributions at large β, showing ac universality in a scaled frequency representation. The diffusion cluster approximation (DCA) and the effective medium approximation (EMA), *solid and dashed lines* respectively, are also shown. *Dots* mark a line with slope unity, i.e. a linear frequency dependence, as the limiting behaviour at high frequencies. Reproduced from [94] with permission

characterized by disorder only at a macroscopic scale, which might apply for crystalline ionic conductors. In this case, both the diffusion cluster approximation and the effective medium approximation results in the same expression, $ln\tilde{\sigma} = (j\omega/\tilde{\sigma})$, for the frequency dependence of the ac conductivity.

The random barrier model accounts for a universal frequency dependence of the ac conductivity in the extreme disorder limit, but no rigorous proof of this behavior exist. In fact, the RBM scaling function is close to, but rarely identical to those of experiments. Experimental data often show deviations for the claimed ac universality that are not addressed by the model [43, 48]. Even assuming ac universality, there remain also other important problems not able to address by the model: [33, 94]

- In the diffusion cluster approximation, it is necessary to characterize more precisely the diffusion cluster and its dimension, either by independent simulations or by using analytical arguments.
- It is necessary to determine how realistic is the approximation made by linearizing a hopping model with random site energies and Fermi statistics.
- Is ac universality also obtained, at least in some particular cases, by solving the master equation in Eq. (2.72) without assuming the condition of symmetric hopping?
- The RBM does not deal with the well-known mixed alkali-effect, as well as the observed changes in activation energies when changing the concentration of mobile ions in glasses (see Chap. 4 for a description of these experimental facts). The simplest models accounting for these effects are hopping systems with site

exclusion [97], i.e. where there can be at most one ion at each site, but a conclusive picture of the scaling properties of this type of models remains to be established.
- It is important to clarify how the scaling function and time-temperature superposition are affected by including Coulomb interactions in hopping models [98].
- The RBM predicts characteristic length-scales in ionic glasses to be larger than the values of order 1 Å that have been determined from experimental data [99]. It has been proposed that the reason for this discrepancy is that ion diffusion in glasses takes place by a vacancy mechanism [100], but further studies are needed to clarify this issue.

2.5.2 *The MIGRATION Concept*

The so called MIGRATION concept (MC) [41] is an evolution of the previously developed "Jump Relaxation Model" (JRM) [37] and "Concept of Mismatch and Relaxation" (CMR) [101] by Klaus Funke. The acronym stands for MIsmatch Generated Relaxation for the Accommodation and Transport of IONs. As mentioned in previous section, the dynamics of mobile ions can be expressed in terms of time correlation functions such as the velocity autocorrelation function, $\langle v(0)v(t)\rangle$. Its normalised integral, $W(t)$, which is often called the time-dependent correlation factor, represents the probability for the ion to be (still or again) at its new position after a hop (see Fig. 2.16). Note that, while $W(0)$ is unity by definition, its limiting value at long times, $W(\infty)$, is just the fraction of "successful" hops.

Under the assumption that the cross terms in the velocity correlation function of the hopping ions, $\left\langle \sum_{i,j} v_i(0)v_j(t) \right\rangle$, may be neglected, i.e. $\left\langle \sum_{i,j} v_i(0)v_j(t) \right\rangle = N\langle v(0)v(t)\rangle$, then $\sigma^*_{hop}(\omega)$ becomes proportional to the Fourier transform of the time derivative of $W(t)$ (see Eqs. (2.40–2.43)), denoted by $\dot{W}(t)$. Introducing $W_s(t) = W(t)/W(\infty)$, Eq. (2.40) can be written as [41]

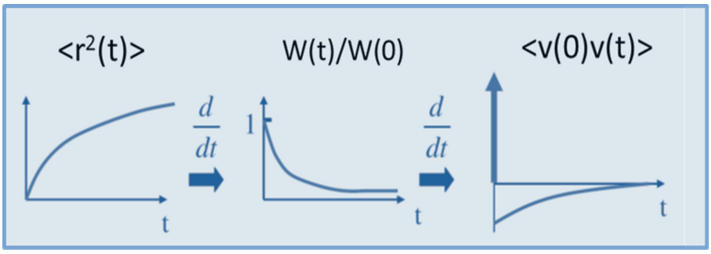

Fig. 2.16 Sketch of the time dependence of the mean square displacement, correlation factor in the MIGRATION concept, and the velocity autocorrelation function of hopping ions, showing the relationships between them. Figure adapted from reference [102]

$$\sigma^{*}_{hop}(\omega)/\sigma(0) = 1 + j\omega \int_0^\infty [W_s(t) - 1] e^{-j\omega t} dt. \tag{2.75}$$

In the physical picture conveyed by the MIGRATION concept, it is emphasized the mismatch introduced by any hop of an ion, the resulting relaxation (rearrangement) of the neighbourhood and, as a consequence of the relaxation, the accommodation (stabilisation) of the ion at its new position. Once accommodation at the new site is achieved, an elementary step of macroscopic transport is completed by the ion. In this model treatment, a simple set of rules is introduced in order to describe the essence of the ion dynamics in terms of a physical picture of the most relevant elementary processes. The rules are expressed in terms of three coupled rate equations, which form the basis for deriving frequency-dependent model conductivities as well as mean square displacements. The set of rules that constitute the MIGRATION concept are:

$$-\frac{\dot{W}(t)}{W(t)} = -B\dot{g}(t), \tag{2.76}$$

$$-\frac{\dot{g}(t)}{g(t)} = \Gamma_0 W(t) N(t), \tag{2.77}$$

$$N(t) = N(\infty) + [\mathrm{B}g(t)]^{\lambda}, \tag{2.78}$$

In these equations, $g(t)$ represents a normalised mismatch function, taking values $g(0) = 1$ and $g(\infty) = 0$. This mismatch function describes the decay of the (normalised) distance between the (new) position of the "central" ion and the position where its neighbours expect it to be. The mismatch created by the hop of the "central" ion is experienced by an effective number of neighbours, $N(t)$, a function that may depend on time. Γ_0 is the elementary hopping rate, while B and λ are parameters. In Eq. (2.76), the rates of relaxation along the single-particle route, with the ion hopping backwards, and on the many-particle route, with the other ions rearranging, are both proportional to the same driving force, $g(t)$, and hence proportional to each other (see Fig. 2.17). According to Eq. (2.77), the rate of decay of $g(t)$, is proportional to the driving force $g(t)$, to the elementary hopping rate, Γ_0, and to the number function, $N(t)$. It is also proportional to $W(t)$, since the mobile neighbours perform correlated forward–backward jumps in the same fashion as the "central" ion does.

Model conductivity spectra can be obtained from Eqs. (2.76–2.78) and compared with experimental ones [104]. The shape of the conductivity spectra depends on the value of the parameters B and λ, but it is not clear what their physical significance is. Figure 2.18 shows frequency-dependent conductivities of the supercooled glass-forming melt $0.4Ca(NO_3)_2$–$0.6KNO_3$ (CKN) at 393 K and 353 K, respectively, above and below the coupled-to-decoupled transition

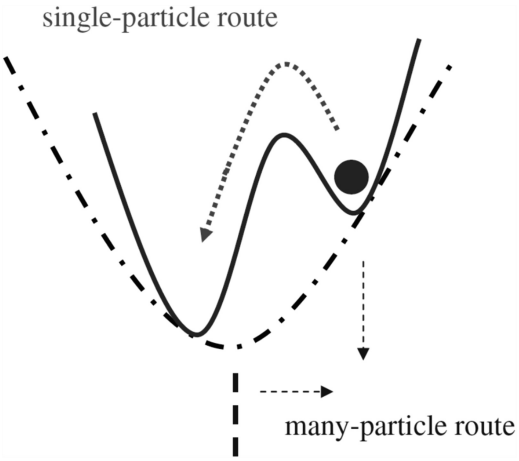

Fig. 2.17 Sketch of the MIGRATION concept. The backward hop of the ion implies the possible relaxation on the single-particle route, while the shift of the caged potential indicates the possible relaxation along the many-particle route. The *solid line* represents the effective potential experienced by the hopping ion. Reproduced from [103] by permission

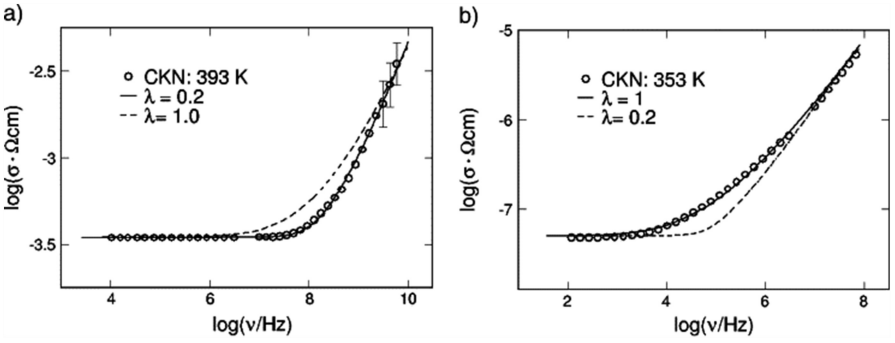

Fig. 2.18 Real part of the conductivity vs frequency of a supercooled melt of CKN (**a**) above and (**b**) below the coupled-to-decoupled transition temperature. In the model curves, the value of the parameter λ is found to change from 0.2 to 1.0. Reproduced from [104] by permission

temperature reported at 378 K [105]. It can be observed that both conductivity isotherms are well reproduced by the equations of the MIGRATION concept, but different values are found for the parameter λ. At the higher temperature, in the fluid melt, a 'successful' displacement of an individual ion only seems to require suitable movements of its immediate neighbours, and hence there is no need to consider any significant time dependence of their number. At the lower temperature, in the viscous melt, a solid-like conduction mechanism seems to prevail. The system is now decoupled, with mobile ions moving from site to site in a comparatively immobile structure. In such a scenario, long-range Coulomb forces between the

ions become important, the mismatch of a "central" ion exerting dipole forces on its mobile neighbours, thus inducing their rearrangement by suitable hops and thereby reducing the mismatch [41]. More discussion of the MC and relation to experimental data are given in Chap. 4.

2.5.3 The Coupling Model

The Coupling Model (CM) was proposed in 1979 with the purpose of providing a general theoretical treatment of relaxation and diffusion in systems where the relaxing or diffusing units are interacting with each other, i.e. the many-body problem of irreversible processes in classical statistical mechanics. Exploring the effect that interaction between the relaxing or diffusing units has on the dynamics ranging from microscopic to macroscopic times and the transport coefficients is the objective of the CM. Surprisingly no such theory or model exists at least before 1979 despite the fact that most condensed matter including glass-forming liquids, glasses and ionic conductors are interacting systems, and relaxation and diffusion are the major properties of interest.

The first version of the Coupling Model (CM) [34, 106–108] on relaxation of interacting systems was published in 1979. In retrospect, this model is based on semiclassical quantization of nonlinear Hamiltonian mechanics, i.e. classical chaos [109–113]. The interacting system is semiclassically quantized and the energy levels distribution is described by Wigner's statistical theory [114–116]. This theory of Wigner originated from his idea that the complex Hamiltonians of many-body interacting systems (in the original case considered by Wigner, it is that of heavy atom nuclei such as uranium) could be approximated by a random Hamiltonian representing the probability distribution of individual Hamiltonians for the purpose of finding the energy levels. This idea was then further developed with advances in random matrix theory and statistics [117]. For systems invariant under time reversal, it is given by the Gaussian Orthogonal Ensemble (GOE) in random matrix theory. It makes sense to use GOE because it has been shown to apply to a variety of atomic, molecular, nuclear systems. [113–117] In GOE, the distribution of level spacings E is given by the expression, $p(E/D) = (\pi/2)(E/D)\exp\left[-(\pi/4)(E/D)^2\right]$, and D is the average spacing. In the absence of interactions, the level spacings follow the Poisson distribution, drastic different from the GOE (see Fig. 2.19). GOE has the characteristic linear dependence of $p(E/D) \propto E/D$ which originates from energy level repulsions, and this dependence holds up to a cut-off high energy, E_c. When considering relaxation and diffusion, frequency ω or time t varies over many orders of magnitude, and $\log\omega$ or $\log t$ is the appropriate variable. Since energy E correspond to ω or time $1/t$, we replot $p(E/D)$ vs. $\log(E/D)$ in Fig. 2.20, and put $\log(\omega/\omega_c)$ or $\log(t/t_c)$ under $\log(E/D)$, as label of the abscissa, to indicate the corresponding variables when considering relaxation. Like D, the magnitudes of $\omega_c = E_c/\hbar$, where $\hbar$ is the Planck's

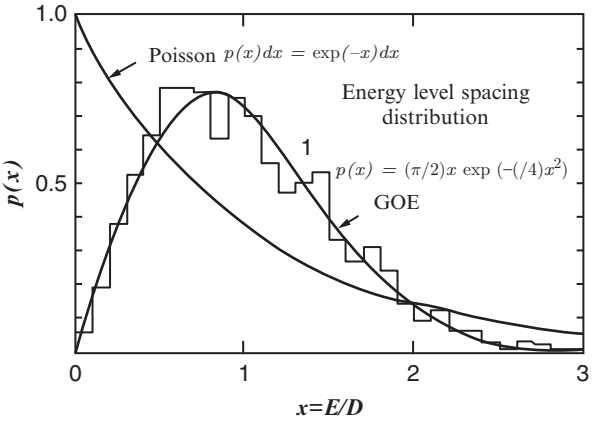

Fig. 2.19 A Wigner distribution fitted to the spacing distribution of 932 s-wave resonances in the interaction $^{238}\mathrm{U} + \mathrm{n}$ at energies up to 20 keV. The Poisson distribution is shown for contrast

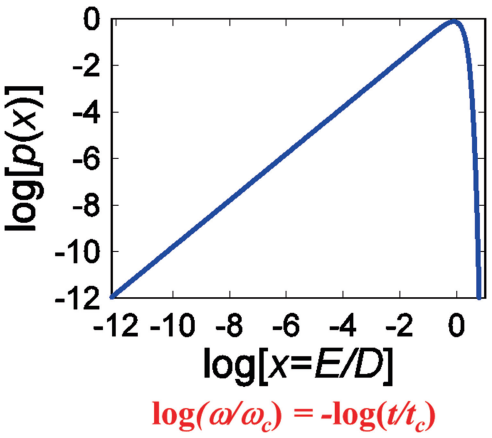

Fig. 2.20 Replotting the GOE in Fig. 2.19 as log vs. log

constant, and t_c depends on the interaction strength determined by the potential of interaction, and it is insensitive to temperature or pressure. Stronger is the interaction strength, larger is D and ω_c and shorter is t_c.

The results given above brings out the physics that interactions has no effect on relaxation and diffusion at frequencies higher than ω_c or at times shorter than t_c. This is because the linear dependence of the level spacing distribution on E no longer holds for $E > E_c$, which corresponds to times shorter than $t_c \equiv (\omega_c)^{-1}$. So, if ion-ion interaction is the cause of the non-exponential time correlation function of many-body conductivity relaxation such as that given by the Kohlrausch function of Eq. (2.49), it is ineffective at times shorter than t_c, and the normalized correlation function is simply the one-body exponential function, $\Phi(t) = \exp(-t/\tau_0)$, of Debye in relaxation and of Einstein in Brownian diffusion.

Therefore, in the CM, at times shorter than $t_c \equiv (\omega_c)^{-1}$ the relaxation is a primitive or one-body (single ion) relaxation with constant rate $W_0 \equiv (\tau_0)^{-1}$, and the correlation function is given by $\exp(-t/\tau_0)$. Due to interactions and the onset of

the linear level spacings distribution or correlations between the ions, the many-body relaxation takes over after crossing t_c. It is the response of the GOE energy level structure to the primitive relaxation that is used to account for the many-body relaxation which necessarily slows down its primitive relaxation rate W_0 [106–108]. Calculated by perturbation theory, the response coming from $p(E)$ with the linear dependence on E slows down the relaxation rate W_0 to have the time dependent form of

$$W(t) = W_0(w_c t)^{-n}, \quad t > t_c, \tag{2.79}$$

and the correlation function to have the Kohlrausch form given by Eq. (2.49), for times longer than t_c. The power, n, called the coupling parameter, is a fraction of unity which increases with the strength of interaction. Thus, the relaxation rate of interacting many-body systems is time dependent. It is the primitive relaxation rate, $W(t) = W_0$ for $t < t_c$, and the many-body relaxation rate, $W(t) = W_0(\omega_c t)^{-n}$, when $t > t_c$. This crossover from the primitive to the many-body relaxation rate does not occur necessarily sharply at t_c but rather smoothly in a neighborhood of t_c, so that the correlation function and its derivatives are continuous across t_c. The factor, $\exp\left[-(\pi/4)(E/D)^2\right]$, in $p(E)$ effects the transition between the two rates. Its width parameter D suggests that the width of the neighborhood is of the order of t_c itself, and hence narrow, if there is no other factor like polydispersity of relaxation units entering into the problem. Some of the experimental data to be introduced later show that the crossover is quite sharp. In view of this and in the absence of reliable way to account quantitatively for the narrow crossover, the sharp crossover of the two relaxation rates at t_c is used to generate predictions. The correlation function in Eq. (2.32), $\phi(t)$ obtained from the CM rate equation, $\partial\phi(t)/\partial t = -W(t)\phi(t)$, by integration with $\tau_0 \equiv 1/W_0$ is given by

$$\phi(t) = \exp(-t/\tau_0), \quad t < t_c, \tag{2.80}$$

$$\phi(t) = A \exp\left[-(t/\tau^*)^{1-n}\right], \quad t > t_c, \tag{2.81}$$

and continuity of $\phi(t)$ at t_c leads to the relation,

$$\tau^*(T,P,Q,m,U,\cdots) = [(1-n)(t_c)^{-n}\tau_0(T,P,Q,m,U,\cdots)]^{\frac{1}{1-n}}, \tag{2.82}$$

and

$$A = \exp\{[n/(1-n)](t_c/\tau_0)\}. \tag{2.83}$$

In Eq. (2.82) the dependences of τ^* and τ_0 on temperature T, pressure P, isotope mass m, neutron scattering vector Q, and any other variable U are written out explicitly to show how the two are related.

When τ_0 is much longer than t_c, $A \to 1$, and

$$\phi(t) = \exp\left[-(t/\tau^*)^{1-n}\right], \quad t > t_c, \tag{2.84}$$

$$\tau^*(T,P,Q,m,U,\cdots) = [(t_c)^{-n}\tau_0(T,P,Q,m,U,\cdots)]^{\frac{1}{1-n}} \tag{2.85}$$

There is no difference between Eqs. (2.82) and (2.85) when the CM is used merely to predict the relation between the dependence of the many-body relaxation time τ^* with that of the primitive τ_0 on some variable U. For example if τ_0 has Arrhenius T-dependence with activation energy E_a, then both equations predict that the activation energy of τ is given by $E_a/(1-n)$. From the Q^{-2}-dependence of τ_0, Eq. (2.85) predicts that the τ^* has the $Q^{-2/(1-n)}$-dependence. Thus the CM Eq. (2.85) spawns many predictions to compare with experiments. Quantitatively for the relation between τ_0 and τ^*, the two expressions make some difference particularly when n becomes larger. In that case, Eq. (2.82) should be used when τ_0 is not much longer than t_c for the sake of accuracy, as demonstrated in comparing prediction [118] with molecular dynamics simulation data [119] where n has unusually large value. When using the prediction to deduce quantitatively τ_0 from the experimentally observed τ^* with known values of n and t_c, Eqs. (2.82) and (2.85) leads respectively to $\tau_0 = (t_c)^n(\tau^*)^{1-n}/(1-n)$ and

$$\tau_0 = (t_c)^n(\tau^*)^{1-n}. \tag{2.86}$$

The difference between the two expressions for τ_0 is not large, only a factor 2 for $n = 0.5$, and lesser for smaller values of n. For this reason, Eq. (2.86) is often used.

The significance of the CM equation Eqs. (2.82) and (2.85) is that it makes a connection between the many-body relaxation time τ^* usually endowed with anomalous properties and the primitive one-body relaxation time τ_0, the properties of which are normal and known. Thus, the connection provides falsifiable explanations/predictions of the anomalous properties of τ from the known or familiar properties of τ_0. The connection is made via the Kohlrausch exponent n, and the crossover time t_c. These two parameters of the many-body relaxation naturally are ultimately determined by the interaction potential and its strength.

The Eqs. (2.82) and (2.85) coupled with the Kohlrausch function of the CM spawns many predictions that can be tested by experiments and used to explain anomalous properties. Many such tests and applications are given in Chap. 4. Since it was derived for complex Hamiltonians in general, the predictions form these equations should apply to relaxation and diffusion in interacting many-body systems of many kinds, and the dynamics of ionic conductors is only a special case. Thus, ever since the inception of the CM in 1979, the expected existence of universal relaxation and diffusion properties of interacting many-body systems has led to concurrent explorations of several fields using the two coupled equations (2.84) and (2.85) as the tool [18]. It must be borne in mind that these equations hold strictly for systems in which all relaxation/diffusing units are identical and

monodisperse, and heterogeneity is not introduced by boundaries, randomness, mixing, and etc. If extrinsic heterogeneity is present, these equations have to be modified by incorporating extraneous factors, and the test of applicability of the CM become less precise and direct, but nevertheless can be done. Moreover, the two coupled equations (2.84) and (2.85) strictly apply to the terminal many-body relaxation leading to steady state transport coefficients. Before reaching the terminal relaxation, the dynamics of ions have passed through several stages. The first stage is the dissipation of ions mutually confined in cages through the interionic potential, manifesting as the nearly constant loss (NCL) in $\varepsilon''(\omega)$ and $\sigma'(\omega)$ (see Chap. 4). The caged ion dynamics has no characteristic time and continues with time indefinitely until the onset of the primitive ion relaxation corresponding to ion hop out of the cage singly or independently, which is the second stage. Thereafter, increasing number of ions cooperatively relax continuously with time (this is the third stage), until the maximum number (or length-scale L) of the heterogeneous ion dynamics is reached. The latter is the terminal or primary many-ions relaxation with time correlation function and relaxation time governed by Eqs. (2.84) and (2.85).

The CM does not provide description of the motion of ions in space at the third and the final stage. Notwithstanding, the CM had anticipated that these processes in interacting many-body systems is dynamically heterogeneous by pointing out [120] the analogy of the CM to the heterogeneous process in the solution of the 'Dining Philosophers Problem' in computer science [121], 1 year before the first experimental evidence of dynamic heterogeneity of structural α-relaxation was published [16]. In the CM, dynamic heterogeneity and Kohlrausch non-exponentiality, Eq. (2.84), are regarded as parallel consequences of the cooperative many-body molecular dynamics, but the former is not emphasized in the applications of the CM. Description of the motions as a function of time is best obtained by special experiment techniques like confocal microscopy for colloidal suspensions [17, 122] or by molecular dynamics simulations of ions [123] and especially designed computer simulation method for molecular liquids such as the Dynamic Lattice Liquid Model [124, 125]. Such description is worthwhile as well as pleasing to acquire, but being able to describe motions as a function of time does not necessarily mean that it can explain the anomalous properties of the terminal many-ion relaxation time, τ, while the CM equation can do just that via Eq. (2.85). Ever since it was first derived in 1979, this problem-solving capability of the CM continues to apply in the field of ionic conductivity relaxation and other areas, particularly the dynamics of glass-forming materials and systems [18]. Plenty of examples from ionic conductivity relaxation will be given in Chaps. 4–7.

References

1. L. Landau, E. Lifschitz, *Textbook of Theoretical Physics, Vol. V. Statistical Physics* (Akademie-Verlag, Berlin, 1979).
2. F. Kremer, A. Schönhals (eds.), *Broadband Dielectric Spectroscopy* (Springer, Berlin, 2012), p. 729

3. R. de L. Kronig, J. Opt. Soc. Am. **12**, 547 (1926)
4. H. Kramers, *Atti Del Congr. Internazionale Dei Fis*, 2nd edn. (Bologna Zanichelli, 1927), p. 545
5. C.F. Bohren, Eur. J. Phys. **31**, 573 (2010)
6. J.D. Jackson, *Classical Electrodynamics* (Wiley, New York, 1999)
7. H. Nyquist, Phys. Rev. **32**, 110 (1928)
8. H.B. Callen, T.A. Welton, Phys. Rev. **83**, 34 (1951)
9. G. Williams, J. Fournier, J. Chem. Phys. **104**, 5690 (1996)
10. L. Onsager, Phys. Rev. **37**, 405 (1931)
11. L. Onsager, Phys. Rev. **38**, 2265 (1931)
12. C.J.F. Böttcher, P. Bordewijk, *Theory of Electric Polarization, Vol. II: Dielectrics in Time-Dependent Fields* (Elsevier, Amsterdam/Oxford/New York, 1978)
13. P. Debye, Phys. Z. **13**, 97 (1912)
14. P. Debye, Ber. Deut. Phys. Ges. **55**, 777 (1913)
15. G. Adam, J.H. Gibbs, J. Chem. Phys. **43**, 139 (1965)
16. K. Schmidt-Rohr, H. Spiess, Phys. Rev. Lett. **66**, 3020 (1991)
17. E. Weeks, J. Crocker, A. Levitt, A. Schofield, D. Weitz, Science **287**, 627 (2000)
18. K.L. Ngai, *Relaxation and Diffusion in Complex Systems* (Springer, New York, 2011), p. 835
19. R. Kohlrausch, Ann. Der Phys. Und Chemie **167**, 179 (1854)
20. G. Williams, D.C. Watts, Trans. Faraday Soc. **66**, 80 (1970)
21. G. Williams, D.C. Watts, S.B. Dev, A.M. North, Trans. Faraday Soc. **67**, 1323 (1971)
22. M. Cardona, R.V. Chamberlin, W. Marx, Ann. Phys. **16**, 842 (2007)
23. G. Williams, IEEE Trans. Electr. Insul. **EI-17**, 469 (1982)
24. G. Williams, IEEE Trans. Electr. Insul. **EI-20**, 843 (1985)
25. K. Tsang, K. Ngai, Phys. Rev. E **56**, R17 (1997)
26. K.L. Ngai, J. Habasaki, Y. Hiwatari, C. Leon, J. Phys. Condens. Matter **15**, S1607 (2003)
27. S. Havriliak, S. Negami, J. Polym. Sci. Part C Polym. Symp. **14**, 99 (1966)
28. A. Jonscher, *Dielectric Relaxation in Solids* (Chelsea, London, 1983)
29. K.S. Cole, R.H. Cole, J. Chem. Phys. **9**, 341 (1941)
30. D.W. Davidson, R.H. Cole, J. Chem. Phys. **19**, 1484 (1951)
31. I.M. Hodge, K.L. Ngai, C.T. Moynihan, J. Non-Cryst. Solids **351**, 104 (2005)
32. C. Angell, Annu. Rev. Phys. Chem. **43**, 693 (1992)
33. J. Dyre, T. Schrøder, Rev. Mod. Phys. **72**, 873 (2000)
34. K.L. Ngai, A.K. Jonscher, C.T. White, Nature **277**, 185 (1979)
35. K.L. Ngai, J. Habasaki, C. León, A. Rivera, Z. Phys. Chem. **219**, 47 (2005)
36. C. León, J. Habasaki, K.L. Ngai, Zeitschrift Für Phys. Chemie **223**, 1311 (2009)
37. K. Funke, Prog. Solid State Chem. **22**, 111 (1993)
38. A.K. Jonscher, Nature **267**, 673 (1977)
39. D.P. Almond, A.R. West, R.J. Grant, Solid State Commun. **44**, 1277 (1982)
40. C. Cramer, K. Funke, T. Saatkamp, Philos. Mag. Part B **71**, 701 (1995)
41. K. Funke, Solid State Ionics **169**, 1 (2004)
42. D. Sidebottom, B. Roling, K. Funke, Phys. Rev. B **63**, 024301 (2000)
43. J.C. Dyre, P. Maass, B. Roling, D.L. Sidebottom, Rep. Prog. Phys. **72**, 046501 (2009)
44. D. Sidebottom, Phys. Rev. Lett. **82**, 3653 (1999)
45. C. León, M. Lucia, J. Santamaria, Phys. Rev. B **55**, 882 (1997)
46. C.T. Moynihan, J. Non-Cryst. Solids **172–174**, 1395 (1994)
47. C. Moynihan, Solid State Ionics **105**, 175 (1998)
48. K.L. Ngai, C.T. Moynihan, MRS Bull. **23**, 51 (1998)
49. P.B. Macedo, C.T. Moynihan, R. Bose, Phys. Chem. Glas. **13**, 171 (1972)
50. T.J. Higgins, L.P. Boesch, V. Volterra, C.T. Moynihan, P.B. Macedo, J. Am. Ceram. Soc. **56**, 334 (1973)
51. F.S. Howell, R.A. Bose, P.B. Macedo, C.T. Moynihan, J. Phys. Chem. **78**, 639 (1974)
52. C.T. Moynihan, L.P. Boesch, N.L. Laberge, Phys. Chem. Glas. **14**, 122 (1973)

53. J.R. Macdonald, J. Chem. Phys. **102**, 6241 (1995)
54. B.A. Boukamp, Solid State Ionics **20**, 31 (1986)
55. B. Boukamp, J.R. Macdonald, Solid State Ionics **74**, 85 (1994)
56. C. León, M.L. Lucía, J. Santamaría, Philos. Mag. Part B **75**, 629 (1997)
57. F. Alvarez, A. Alegra, J. Colmenero, Phys. Rev. B **44**, 7306 (1991)
58. K.L. Ngai, J. Chem. Phys. **98**, 6424 (1993)
59. P. Kofstad, T. Norby, *Defects and Transport in Crystalline Solids* (University of Oslo, Oslo, 2007)
60. M.S. Islam, C.A.J. Fisher, Chem. Soc. Rev. **43**, 185 (2014)
61. G. Ceder, MRS Bull. **35**, 693 (2011)
62. L. Malavasi, C.A.J. Fisher, M.S. Islam, Chem. Soc. Rev. **39**, 4370 (2010)
63. Y. Wang, W.D. Richards, S.P. Ong, L.J. Miara, J.C. Kim, Y. Mo, G. Ceder, Nat. Mater. **14**, 1026 (2015)
64. Z. Wojnarowska, M. Paluch, J. Phys. Condens. Matter **27**, 073202 (2015)
65. T. Norby, Mater. Res. Soc. Bull. **34**, 923 (2009)
66. C. Zener, Proc. R. Soc. A Math. Phys. Eng. Sci. **137**, 696 (1932)
67. K. Ngai, Solid State Ionics **105**, 231 (1998)
68. L. Van Hove, Phys. Rev. **95**, 249 (1954)
69. A. Rahman, K.S. Singwi, A. Sjölander, Phys. Rev. **126**, 986 (1962)
70. R. Kubo, J. Phys. Soc. Jpn. **12**, 570 (1957)
71. T. Odagaki, M. Lax, Phys. Rev. B **24**, 5284 (1981)
72. D. Ben-Avraham, S. Havlin, *Diffusion and Reactions in Fractals and Disordered Systems* (Cambridge University Press, Cambridge, 2000), p. 316
73. S. Elliott, Solid State Ionics **27**, 131 (1988)
74. T. Odagaki, M. Lax, Phys. Rev. Lett. **45**, 847 (1980)
75. T. Odagaki, Phys. Rev. B **38**, 9044 (1988)
76. T. Nakayama, Rep. Prog. Phys. **65**, 1195 (2002)
77. T. Ishii, J. Phys. Soc. Jpn. **61**, 924 (1992)
78. T. Ishii, Solid State Ionics **40–41**, 244 (1990)
79. A. Bunde, H. Roman, S. Russ, A. Aharony, A. Harris, Phys. Rev. Lett. **69**, 3189 (1992)
80. E. Bacry, J. Delour, J.F. Muzy, Phys. Rev. E. Stat. Nonlin. Soft Matter Phys. **64**, 026103 (2001)
81. M. Shlesinger, B. West, J. Klafter, Phys. Rev. Lett. **58**, 1100 (1987)
82. T. Geisel, J. Nierwetberg, A. Zacherl, Phys. Rev. Lett. **54**, 616 (1985)
83. J. Habasaki, K.L. Ngai, J. Chem. Phys. **129**, 194501 (2008)
84. J. Habasaki, I. Okada, Y. Hiwatari, Phys. Rev. B **55**, 6309 (1997)
85. A. Blumen, J. Klafter, B.S. White, G. Zumofen, Phys. Rev. Lett. **53**, 1301 (1984)
86. J. Habasaki, I. Okada, Y. Hiwatari, J. Phys. Soc. Jpn. **67**, 2012 (1998)
87. K. Popper, *Conjectures and Refutations: The Growth of Scientific Knowledge* (Routledge Classics, New York, 1963)
88. J.C. Kimball, L.W. Adams, Phys. Rev. B **18**, 5851 (1978)
89. J.C. Dyre, T.B. Schroeder, Phys. Status Solidi **230**, 5 (2002)
90. P.N. Butcher, J. Phys. C Solid State Phys. **7**, 879 (1974)
91. D.L. Stein, C.M. Newman, Phys. Rev. E **51**, 5228 (1995)
92. J.W. Haus, K.W. Kehr, Phys. Rep. **150**, 263 (1987)
93. J.C. Dyre, J. Appl. Phys. **64**, 2456 (1988)
94. T.B. Schrøder, J.C. Dyre, Phys. Chem. Chem. Phys. **4**, 3173 (2002)
95. V. Ambegaokar, B.I. Halperin, J.S. Langer, Phys. Rev. B **4**, 2612 (1971)
96. T. Schrøder, J. Dyre, Phys. Rev. Lett. **84**, 310 (2000)
97. S.D. Baranovskii, H. Cordes, J. Chem. Phys. **111**, 7546 (1999)
98. W. Dieterich, P. Maass, Chem. Phys. **284**, 439 (2002)
99. B. Roling, C. Martiny, K. Funke, J. Non-Cryst. Solids **249**, 201 (1999)
100. J.O. Isard, J. Non-Cryst. Solids **246**, 16 (1999)

101. K. Funke, R.D. Banhatti, S. Brückner, C. Cramer, C. Krieger, A. Mandanici, C. Martiny, I. Ross, Phys. Chem. Chem. Phys. **4**, 3155 (2002)
102. K. Funke, R.D. Banhatti, J. Non-Cryst. Solids **353**, 3845 (2007)
103. K. Funke, R.D. Banhatti, D.M. Laughman, L.G. Badr, M. Mutke, A. Santic, W. Wrobel, E.M. Fellberg, C. Biermann, Zeitschrift Für Phys. Chemie **224**, 1891 (2010)
104. K. Funke, R.D. Banhatti, Solid State Ionics **177**, 1551 (2006)
105. P. Singh, R.D. Banhatti, K. Funke, Phys. Chem. Glas. **46**, 241 (2005)
106. K.L. Ngai, Comment Solid State Phys. **9**, 141 (1980)
107. K.L. Ngai, C.T. White, Phys. Rev. B **20**, 2475 (1979)
108. K.L. Ngai, Comment Solid State Phys. **9**, 127 (1980)
109. M. Gutzwiller, *Chaos in Classical and Quantum Mechanics* (Springer, Berlin, 1990)
110. M.V. Berry, Proc. R. Soc. A Math. Phys. Eng. Sci. **413**, 183 (1987)
111. M. Berry, Phys. Scr. **40**, 335 (1989)
112. O. Bohigas, Chaos Phys. Quantique Chaos Quantum Phys. 87 (1989)
113. O. Bohigas, M.J. Giannoni, C. Schmit, Phys. Rev. Lett. **52**, 1 (1984)
114. E.P. Wigner, *Proceedings of Fourth Canadian Mathematical Congress* (University Toronto Press, Toronto, 1957), p. 174
115. M.L. Mehta, *Random Matrices*, 2nd edn. (Academic, New York, 1991)
116. F.J. Dyson, J. Math. Phys. **3**, 140 (1962)
117. L. Gor'kov, G. Eliashberg, JETP **21**, 940 (1965)
118. K.L. Ngai, S. Capaccioli, J. Phys. Condens. Matter **19**, 205114 (2007)
119. D. Bedrov, G.D. Smith, Macromolecules **39**, 8526 (2006)
120. I.A. Campbell, C. Giovannella (eds.), *Relaxation in Complex Systems and Related Topics* (Springer, Boston, 1990)
121. G. Kolata, Science **223**, 917 (1984)
122. E. Weeks, D. Weitz, Phys. Rev. Lett. **89**, 095704 (2002)
123. J. Habasaki, K.L. Ngai, J. Non-Cryst. Solids **352**, 5170 (2006)
124. T. Pakula, J. Mol. Liq. **86**, 109 (2000)
125. P. Polanowski, T. Pakula, J. Chem. Phys. **117**, 4022 (2002)

http://www.springer.com/978-3-319-42389-0

Dynamics of Glassy, Crystalline and Liquid Ionic Conductors
Experiments, Theories, Simulations
Habasaki, J.; Leon, C.; Ngai, K.L.
2017, XIX, 600 p. 249 illus., 196 illus. in color.,
Hardcover
ISBN: 978-3-319-42389-0